HHS Public Access

Author manuscript

Cell. Author manuscript; available in PMC 2018 January 26.

Published in final edited form as:

Cell. 2017 July 27; 170(3): 522–533.e15. doi:10.1016/j.cell.2017.06.049.

A Genetic Variant Associated with Five Vascular Diseases Is a Distal Regulator of Endothelin-1 Gene Expression

Rajat M. Gupta[1,2,3,8,*], **Joseph Hadaya**[1], **Aditi Trehan**[1], **Seyedeh M. Zekavat**[1], **Carolina Roselli**[1], **Derek Klarin**[1], **Connor A. Emdin**[1], **Catharina R.E. Hilvering**[4], **Valerio Bianchi**[4], **Christian Mueller**[6], **Amit V. Khera**[1,2,3], **Russell J.H. Ryan**[1,5], **Jesse M. Engreitz**[1], **Robbyn Issner**[1], **Noam Shoresh**[1], **Charles B. Epstein**[1], **Wouter de Laat**[4], **Jonathan D. Brown**[7], **Renate B. Schnabel**[6], **Bradley E. Bernstein**[1,5], and **Sekar Kathiresan**[1,2,3,*]

[1]Broad Institute of MIT and Harvard University, Cambridge, MA, USA [2]Cardiology Division, Department of Medicine, Massachusetts General Hospital and Harvard Medical School, Boston, MA USA [3]Center for Genomic Medicine, Department of Medicine, Massachusetts General Hospital and Harvard Medical School, Boston, MA, USA [4]Hubrecht Institute, University Medical Center Utrecht, Utrecht, the Netherlands [5]Department of Pathology, Massachusetts General Hospital and Harvard Medical School, Boston, MA, USA [6]Department of General and Interventional Cardiology, University Heart Center Hamburg-Eppendorf, Hamburg, Germany [7]Division of Cardiovascular Medicine, Vanderbilt University Medical Center, Nashville, TN, USA

Summary

Genome-wide association studies (GWASs) implicate the *PHACTR1* locus (6p24) in risk for five vascular diseases, including coronary artery disease, migraine headache, cervical artery dissection, fibro-muscular dysplasia, and hypertension. Through genetic fine mapping, we prioritized rs9349379, a common SNP in the third intron of the *PHACTR1* gene, as the putative causal variant. Epigenomic data from human tissue revealed an enhancer signature at rs9349379 exclusively in aorta, suggesting a regulatory function for this SNP in the vasculature. CRISPR-edited stem cell-derived endothelial cells demonstrate rs9349379 regulates expression of endothelin 1 (*EDN1*), a gene located 600 kb upstream of *PHACTR1*. The known physiologic effects of *EDN1* on the vasculature may explain the pattern of risk for the five associated diseases. Overall, these data illustrate the integration of genetic, phenotypic, and epigenetic analysis to identify the biologic mechanism by which a common, non-coding variant can distally regulate a gene and contribute to the patho-genesis of multiple vascular diseases.

Graphical abstract

[*]Correspondence: rgupta@broadinstitute.org (R.M.G.), skathiresan1@mgh.harvard.edu (S.K.) http://dx.doi.org/10.1016/j.cell.2017.06.049.

[8]Lead Contact

Supplemental Information: Supplemental Information includes seven figures and four tables and can be found with this article online at http://dx.doi.org/10.1016/j.cell.2017.06.049.

Author Contributions: Conceptualization, R.M.G. and S.K.; Methodology, R.M.G., J.H., C.B.E., C.R.E.H., V.B., R.J.H.R., J.M.E., C.E., and W.d.L.; Investigation, R.M.G., J.H., A.T., C.M., C.R.E.H., V.B., N.S., C.R., C.E., D.K., A.K., S.M.Z., R.B.S., and R.I.; Writing – Original Draft, R.M.G. and S.K.; Writing – Review & Editing, R.M.G., J.H., J.M.E., J.B., and S.K.; Funding Acquisition, S.K. and W.d.L.; Resources, S.K., B.E.B., and W.d.L.; Supervision, S.K., B.E.B., and W.d.L.

A common sequence variant that perturbs long-range enhancer interactions mediates risk for different vascular diseases.

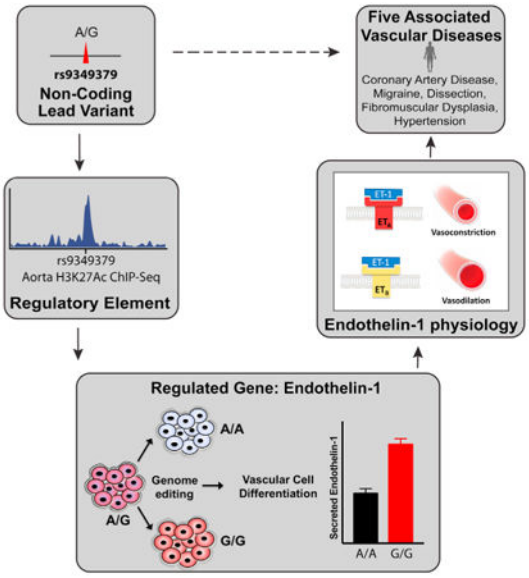

Introduction

Coronary artery disease (CAD) remains the leading cause of morbidity and mortality worldwide and is heritable. Genome-wide association studies (GWASs) have mapped >65 genomic loci for CAD, with most residing in non-coding sequence (CARDIoGRAMplusC4D Consortium et al., 2013; Myocardial Infarction Genetics and CARDIoGRAM Exome Consortia Investigators et al., 2016; Nikpay et al., 2015; Webb et al., 2017). At many of these loci, the causal DNA sequence variant, gene, and mechanism remain undetermined. The diversity of cell types potentially involved in CAD pathogenesis (endothelial cells, smooth muscle cells, monocytes, and cells of the adaptive immune system) complicates functional determination of the underlying causal mechanisms. As a result, successful translation of SNP associations into causal genes and biologic pathways has been confined to a small subset of GWAS loci in CAD (Bauer et al., 2015; Musunuru et al., 2010; Nurnberg et al., 2015).

The identification of causal genes for CAD has relied on connecting a variant with genetic expression differences, which is now broadly available through the GTEx consortium (GTEx Consortium, 2013). Though there is mounting evidence that many GWAS variants regulate transcription (Maurano et al., 2012; Roadmap Epigenomics Consortium et al., 2015; Schaub et al., 2012), these data are not sufficient to identify the causal gene(s) at a locus given the large number of *cis*-expression quantitative trait locus (eQTL) relationships that exist for many variants. Though disease-associated loci are often named by the closest gene to the variant, or the gene with the strongest eQTL, neither can identify a causal gene with certainty.

Here we focus on a genomic locus associated with CAD and four other vascular disorders. Common DNA sequence variants at 6p24 have shown genome-wide significant association with early-onset myocardial infarction (Myocardial Infarction Genetics Consortium et al., 2009), CAD (CARDIoGRAMplusC4D Consortium et al., 2013; Nikpay et al., 2015), coronary artery calcification (O'Donnell et al., 2011), migraine headache (Anttila et al., 2013), cervical artery dissection (Debette et al., 2015), fibromuscular dysplasia (Kiando et al., 2016), and hypertension (Surendran et al., 2016), a constellation of diseases suggesting an effect on vascular function. The associated variants at 6p24 lie within the third intron of the gene encoding phosphatase and actin regulatory protein 1 (*PHACTR1*), nominating *PHACTR1* as the effector gene given its physical proximity. In support of this hypothesis, an association exists between risk genotype and *PHACTR1* expression in arterial samples (Aguet et al., 2016; Beaudoin et al., 2015), and *PHACTR1* function is linked with atherosclerosis-relevant phenotypes, such as angiogenesis (Jarray et al., 2011), extracellular matrix protein production (Jarray et al., 2015), and inflammation (Reschen et al., 2016) in vitro. Despite these data, the causal gene at the 6p24 locus remains uncertain. Furthermore, the mechanism that links the causal variant to gene expression at this locus is not known. To dissect how the 6p24 locus affects vascular disease risk, we utilized genetic and epigenomic approaches to identify the causal variant in the locus, the gene(s) regulated by the variant, and the mechanism by which the DNA variant affects the gene.

Results

Fine Mapping Prioritizes a Causal Variant at 6p24

CAD GWASs have identified association between a group of variants in linkage disequilibrium at 6p24 and several diseases. Sequencing at the locus in a French-Canadian cohort has prioritized an intronic variant in this region (Beaudoin et al., 2015). We conducted genetic fine mapping using the data from the CARDIOGRAMplusC4D Consortium (194,427 individuals), and we imputed SNP associations from the 1000 Genomes Project (Figure 1A). Imputation-based fine mapping combines summary level data from the large-scale CARDIOGRAMplusC4D analysis with linkage disequilibrium estimation from a reference set of similar ancestry. This approach can refine the association signal at a previously identified locus (Yang et al., 2012). The strongest association was for a single variant, rs9349379, with an association of 1.81×10^{-42} (odds ratio [OR] = 1.14), far exceeding the association signal for the next most highly associated SNP, rs78145402 (OR = 1.08, 4.69×10^{-17}).

We next conducted a conditional analysis at the 6p24 locus to determine if there exists an association independent of the sentinel SNP. This conditional analysis, after adjusting for rs9349379, showed no evidence of a second independent CAD/myocardial infarction (MI) association at this locus (Figure S1). The Probabilistic Identification of Causal SNPs (PICS) algorithm (Farh et al., 2015) also identifies rs9349379 as the causal SNP, given the haplotype structure at the locus, with greater than 99% probability (Table S1). Thus, statistical evidence prioritizes rs9349379 as a likely causal SNP for the multiple vascular disease associations at this locus.

Phenome-wide Analysis Confirms Vascular-Specific Effect of Causal 6p24 SNP

Phenome-wide association studies (PheWASs) enable unbiased assessment of the relationship between a given variant and a broad range of human disease phenotypes. This approach is particularly useful for a variant, such as rs9349379, with known impact on several diseases. We conducted a PheWAS for this variant in the UK Biobank using individual-level data from 112,338 individuals of European ancestry. The UK Biobank PheWAS confirmed the previously published associations for CAD and migraine headache (Figure 1B; CAD $p = 1.16 \times 10^{-11}$; migraine $p = 0.000717$).

The pattern of association is striking as the minor allele at rs9349379 (G, 36% frequency) leads to increased risk for CAD and coronary calcification but decreased risk for four conditions (migraine headache, cervical artery dissection, fibromuscular dysplasia, and hypertension). Analysis for association between rs9349379 and cardiovascular risk factors confirmed the previously reported association with systolic blood pressure, but no relationship with lipid concentrations, weight, diabetes, or other related measures (Figure S1B, data obtained from analysis of multiple studies listed in Table S3). There was no significant association of rs9349379 with any other diseases in the UK Biobank PheWAS (Figure S1C).

Given the association of rs9349379 with vascular phenotypes, we next determined its relationship with relevant sub-phenotypes. First, in the UK Biobank, we investigated whether the rs9349379 genotype was associated with a measure of arterial stiffness. Arterial stiffness index was measured in the upper extremity using a digital sensor attached to the participant's digit. In 38,817 participants of European ancestry, the G allele at rs9349379 was associated with decreased arterial stiffness index, with $\beta = -0.077$ (95% confidence interval [CI]: −0.034, −0.119), $p = 0.0004$. Second, we used data from a meta-analysis conducted by the Cohorts for Heart and Aging Research in Genomic Epidemiology (CHARGE) Consortium to quantify the effect of rs9349379 on endothelium-dependent flow-mediated vasodilation (FMD). Flow-mediated vasodilation is a standardized assay of endothelial cell function evoked following brief occlusion of the brachial artery (Corretti et al., 2002). Brachial artery flow-mediated vasodilation was measured in 16,662 participants using ultrasound-guided measurement of brachial artery diameter before and immediately following brief occlusion of the vessel by suprasystolic inflation of a blood pressure cuff. The G allele at rs9349379 was associated with decreased flow-mediated vasodilation ($\beta = -0.1209$ [95% CI: −0.5535, −0.6188], $p = 0.004$). Flow-mediated vasodilation is provoked by shear stress on the endothelium and subsequent dilation in response to vasoactive peptides generated by endothelial cells (Sorensen et al., 1995). In aggregate, these genetic data suggest a role for rs9349379 in human endothelial cell function, and our subsequent experiments prioritized the use of endothelial cells to characterize underlying mechanisms.

A Vascular-Specific Regulatory Region at rs9349379

Non-coding variants often affect gene expression by altering the function of enhancer elements, which can control cell-type-specific gene expression programs. Prior studies have used overlap with enhancer elements to prioritize a cell or tissue type for functional analysis of GWAS loci (Farh et al., 2015; Ren and Yue, 2015). In pursuit of a tissue or cell in which

rs9349379 has relevant regulatory function, we examined the occupancy of a histone mark associated with enhancer activity (H3K27Ac) at the locus in all tissues and cell types annotated in the Encyclopedia of DNA Elements (ENCODE) project (ENCODE Project Consortium, 2012). However, there was no detectable H3K27Ac signal at this locus in these datasets (Figure 2A). Notably, vascular tissues were not included in the ENCODE catalog of chromatin states. The newly released ENCODE phase 3 data, however, includes four aortic artery samples. In these aortic samples, a strong enhancer signal overlies rs9349379 (Figure 2B), spanning 1 kb. Of these aorta samples, two were homozygous major (A/A) at rs9349379, one heterozygous (A/G), and one homozygous minor (G/G). All four demonstrate robust H3K27 acetylation at rs9349379 (Figure S2). These data suggest a gene regulatory function exists at this locus in vascular tissue.

Targeted Deletion at the 6p24 Regulatory Element Increases *EDN1* Expression in Vascular Cells

To determine the target gene of the regulatory element at rs9349379, we performed genome-editing experiments inpluripotent stem cells, and we differentiated these cells into two vascular cell types: endothelial cells (ECs) and vascular smooth muscle cells (VSMCs). First, we deleted an 88-bp region at rs9349379 in an induced pluripotent stem cell (iPSC) line using CRISPR/Cas9 with flanking single-guide RNAs (sgRNAs) (Figure 3A). High-efficiency sgRNAs were designed, constructed, and tested for nuclease activity as previously described (Peters et al., 2013). The highest efficiency sgRNAs were nucleofected into iPSCs, and three clones with a bi-allelic 88-bp deletion (Δ88) were generated from a total of 384 screened clones (Figure S3A). These clones, along with three unedited wild-type clones that had also been exposed to the CRISPR/Cas9 complex, were expanded and differentiated into ECs and VSMCs as previously described (Patsch et al., 2015). In both iPSC-derived ECs and VSMCs, loss of the 88 bp flanking rs9349379 resulted in higher expression of the endothelin-1 (*EDN1*) gene compared with wild-type lines (Figure 3B).

Expression of five other genes in the 1-Mb region surrounding rs9349379, including *PHACTR1*, did not differ significantly for either cell type. There was no differential gene expression between wild-type (WT) and Δ88 iPSCs differentiated to a non-vascular cell type, neural crest progenitor cells (Figure S3B). Though *EDN1* expression was differentially regulated in both ECs and VSMCs, there was a 50-fold higher expression in ECs (Figure S3C). We therefore focused further experiments to characterize *cis* regulation by rs9349379 in ECs.

To determine if the *cis* regulation of *EDN1* by the 6p24 regulatory element was present in a different pluripotent cell line, we edited an embryonic stem cell (ESC) line as well. ESC-derived ECs confirmed the regulatory effect, and Δ88 ESC-ECs demonstrated higher expression compared with WT ESC-ECs (Figure 3C; $p = 0.0004$). In ECs, *EDN1* is dynamically upregulated in response to inflammatory stimuli (Yoshizumi et al., 1990). We incubated the WT and Δ88 iPSC-derived ECs with inter-leukin-1α (IL-1α), a potent inflammatory stimulus that induces *EDN1* expression. Stimulation with IL-1α increased *EDN1* expression both in WT and D88 ECs at the mRNA (Figure 3D; $p = 0.005$) and protein levels (Figure 3E; $p = 0.0004$).

These data demonstrate that deletion of a small region of apparent regulatory DNA at rs9349379 results in increased *EDN1* expression and endothelin-1 (ET-1) protein production in ECs and to a lesser extent in VSMCs.

CRISPR/Cas9-Generated Allelic Series at rs9349379 Validates the Regulatory Effect on *EDN1* Expression

To determine if the effect on *EDN1* gene expression is specifically mediated by a genotype at rs9349379, we generated isogenic stem cell lines that were either homozygous major (A/A)or homozygous minor (G/G). Homologous recombination (HR) with CRISPR/Cas9 genome editing proved to be inefficient, due to a lack of high-efficiency sgRNAs in this AT-rich region of the genome and an inability to inactivate the sgRNA once HR successfully occurred. We tested several approaches to improve the efficiency of HR, including use of multiple sgRNAs in the locus, SCR7 inhibitors (Maruyama et al., 2015), and Cpf1 nucleases (Zetsche et al., 2015); however, in screening over 2,500 colonies, we were only able to recover two clones with successful HR without other insertions or deletions (indels) (Figures S4A and S4B). The only successful approach required two rounds of genome editing: first to generate a cell line with protospacer adjacent motif (PAM) sites at the SNP with HR and second to generate the allelic series (Paquet et al., 2016) (Figure 4A). Using this approach, 15% of clones had the appropriate genotype with no additional edits beyond the 1-bp change (Figure S4C). Three clones from each genotype (A/A and G/G) were selected for expansion and differentiation to ESC-ECs. RNA sequencing (RNA-seq) was conducted on the six samples to identify *cis*-and *trans*-regulatory effects of rs9349379. A total of 173,259 transcripts were analyzed. We found 279 differentially expressed (false discovery rate [FDR] < 0.05) transcripts, with clustering of samples according to rs9349379 genotype as expected (Figure 4B). The majority of these differentially expressed transcripts had log2 fold changes <1.5 (243/279,87%; Figure S4D). Gene set enrichment analysis of the differentially expressed genes showed strong enrichment for blood vessel development (FDR = 1.64×10^{-10}), vasculature development (FDR = 2.98×10^{-10}), and blood vessel morphogenesis (FDR = 2.21×10^{-9}).

EDN1, a gene over 600 kb distal to rs9349379, was the only differentially regulated gene within 2 Mb of rs9349379 (Figure 4C). The differentially regulated genes included several mediators of vascular wall integrity and structure, such as *COL4A1*, *COL3A1*, and *FN1* (Figure S4E), which may be downstream effects of increased *EDN1* expression in the G/G ESC-ECs (Amiri et al., 2004; Shi-Wen et al., 2001). RNA-seq was also conducted in six WT and six Δ88 cells, and, of the 173,259 analyzed transcripts, there were 423 differentially regulated genes (Figure S4F). There was significant overlap in the gene set enrichment analysis represented by these differentially regulated genes and those from RNA-seq of the A/A and G/G ESC-ECs. The top pathways were also blood vessel development (FDR = $2.6 \times 10\sim^{7}$) and blood vessel morphogenesis (FDR = 2.6×10^{-7}). In RNA-seq from both the deletion and allelic series ECs, the regulatory effects of rs9349379 localized to vascular development pathways, and they may be explained by the *cis*-regulatory effect on *EDN1* expression.

The qPCR confirmed the differential gene expression seen by RNA-seq, and it demonstrated a *cis*-regulatory effect of genotype at rs9349379 on *EDN1* expression, with the minor allele driving increased *EDN1* expression (Figure 4D; $p = 7.59 \times 10^{-7}$). There was a significant difference in TBC1D7 expression by qPCR ($p = 1.75 \times 10^{-5}$); however, this was not seen in the RNA-seq quantification from separately differentiated cells or the Δ88 deletions. The homozygous minor ESC-ECs also produced more ET-1 protein in the cell-free supernatants at 24 hr in the presence or absence of IL-1α stimulation (Figure 4E; unstimulated $p = 2.12 \times 10^{-5}$ and IL-1α stimulated $p = 0.0006$). To determine the regulatory effect in another vascular cell type, the A/A and G/G ESC lines were differentiated into VSMCs. *EDN1* was the only differentially expressed transcript in the 6p24 locus (Figure 4F; $p = 0.012$) in VSMCs; however, the level of *EDN1* expression was 50-fold lower in VSMCs than in ECs.

Very Low Contact between EDN1 and rs9349379 by Three-Dimensional Chromatin Structure

One possible mechanism by which the distal regulatory element at rs9349379 affects *EDN1* expression is direct contact with the *EDN1* promoter site. Chromatin loops regulate gene expression by positioning distal enhancers in proximity to target genes (Deng et al., 2012; Dowen et al., 2014). To measure the three-dimensional (3D) chromatin topology in this region, circularized chromosome conformation capture sequencing (4C-seq) assays were performed in human coronary artery ECs. 4C-seq revealed a very low contact probability and no evidence for a focal loop between rs9349379 and the *EDN1* promoter (Figure 5A). The *EDN1* promoter contacts multiple sites extending up to 500 kb in both the 3′ and 5′ directions. 4C-seq from the rs9349379 site demonstrated a smaller contact region that extended from chr6:12,690,000–13,350,000. There was a possible area of overlap intergenic to *EDN1* and *PHACTR1* (Figure 5A). Notably, this region featured high levels of H3K27Ac signal in ECs, consistent with a super enhancer (Figure 5B). Super enhancers are large regions of *cis*-regulatory DNA that span up to 12.5 kb, amass large quantities of coactivator proteins, and control cell-type-specific gene expression programs (Parker et al., 2013; Whyte et al., 2013). The common contact region contains four distinct peaks of H3K27Ac signal. Reporter assays with each of these four sites cloned into an SV40-driven luciferase plasmid demonstrated that each *cis* element possessed strong enhancer activity in 293T cells (2- to 12-fold luciferase induction) compared with SV40-promoter sequence alone (Figure 5C). The same chromatin structure was seen in 4C-seq from aortic ECs, iPSC-derived ECs, aortic VSMCs, and primary human monocytes (Figure S5). The significance of these long-range chromatin loops in the regulation of *EDN1* merits further study, but they suggest that the regulatory effect of rs9349379 on *EDN1* is not through traditional enhancer-promoter interactions.

Minor Allele G at rs9349379 Increases Plasma Levels of Big ET-1 in Healthy Subjects

We next tested the effect of genotype at rs9349379 on plasma levels of Big ET-1. The pro-peptide Big ET-1 is the larger precursor product of *EDN1* transcription, and it is secreted and cleaved into the active ET-1 peptide. The 21-amino acid active ET-1 peptide is quickly degraded in vivo; however, the Big ET-1 pro-peptide is more stable and, therefore, measured more reliably in human plasma samples (Woods et al., 1999). Given the effect on *EDN1* expression in genome-edited ECs, we postulated that Big ET-1 levels would be higher in

individuals with the minor allele at rs9349379. We limited our analysis to healthy individuals, given previous reports of alterations in ET-1 levels in patients with pulmonary hypertension and heart failure. From the Partners Biobank cohort, patients with a Charlson Comorbidity Score of 0 and no anti-hypertensive medication use were selected for analysis. A total of 99 plasma samples were obtained, with 33 samples of each genotype at rs9349379 (A/A, A/G, G/G). We found a significant association between G genotype at rs9349379 and higher Big ET-1 levels using an additive model of regression (Figure 6; $p = 0.00136$). There was no significant effect of sex on ET-1 expression (Figure S6; $p = 0.26$). This analysis provides further support in human samples of the association between rs93493979 and the vasoactive ET-1 peptide.

Discussion

A New Mechanism of Regulation for Five Vascular Diseases

The 6p24 locus is linked to five vascular diseases through common variant association studies. Here we identify the causal variant and gene in vascular tissue using the integration of genetic fine mapping, epigenomic profiling, and CRISPR/Cas9 genome editing. We show the allele-specific regulation of *EDN1* expression in pluripotent stem cell lines with CRISPR/Cas9-mediated bi-allelic deletions, an isogenic allelic series generated through two-step HR, and direct measurement of ET-1 protein in human plasma samples.

ET-1, the protein product of the *EDN1* gene, is a 21-amino acid peptide originally discovered in the supernatant of cultured aortic ECs. It functions as the most potent, longest-lasting vasoconstrictor in humans, and it has unrelated roles in neural crest development and regulation of salt balance in the renal collecting ducts (Pollock, 2010). ET-1 is primarily produced by ECs, though it is secreted abluminally toward underlying smooth muscle cells (Wagner et al., 1992). It acts in a paracrine fashion to promote atherosclerotic plaque development through VSMC-mediated vasomotor constriction, remodeling, and proliferation (Amiri et al., 2004; Li et al., 1994; Schiffrin, 2005). Of note, DNA variants proximal to the promoter of *EDNRA,* encoding Endothelin A (ET_A) receptor (one of two receptors for ET-1), show genome-wide significant association with CAD (Figure S7).

Our data indicate that increased endothelial production of ET-1 and subsequent binding to the ET_A receptor promotes atherosclerosis. This hypothesis has been experimentally validated in earlier studies. Endothelial-specific overexpression of *Edn1* in $Apoe^{-/-}$ mice led to increased atherosclerosis (Li et al., 2013). Selective ET_A antagonists have been shown to retard the development of atherosclerosis in western-type diet-fed $Apoe^{-/-}$ mice and hamsters (Barton et al., 1998; Kowala et al., 1995).

In addition to CAD, there are four additional vascular disease associations at the 6p24 locus. The G allele at rs9349379 is associated with decreased risk for migraine headache, cervical artery dissection, and fibromuscular dysplasia—three diseases that co-occur epidemiologically (Olin et al., 2014; Pezzini et al., 2005; Rubinstein et al., 2005). Migraine headache is associated with intracranial and meningeal vasodilation (Asghar et al., 2011; Bolay et al., 2002). Our data are consistent with this physiology, as the G allele at rs9349379 results in higher *EDN1* expression, increased ET-1 binding to the ET_A receptor on VSMCs,

vasoconstriction, and, therefore, reduced risk of migraine headache. At present, little is known about the pathophysiology of cervical artery dissection or fibromuscular dysplasia, and the precise relationship of either disease with vascular tone is uncertain. In addition to vasoconstriction, other effects of ET-1 on VSMCs include proliferation (Hirata et al., 1989), extracellular matrix (ECM) production (Amiri et al., 2004; Shi-Wen et al., 2001), and fibrosis (Xu et al., 2004). The genetic data suggest the shared pathophysiology of migraine, dissection, and fibromuscular dysplasia may occur through one or more of these downstream effects of ET-1, though this requires further investigation.

Finally, the association of the G allele with lower systolic blood pressure (Surendran et al., 2016) may be explained by the action of ET-1 on the second endothelin receptor, ET_B. In contrast to the coronary arteries where ET_A receptors predominate, ET_B receptors are more abundant in the large systemic arteries (Bacon et al., 1996). ET-1 binds to ET_B receptors on ECs in large vessels, triggering endothelium-dependent vasodilation through the production of nitric oxide, prostacyclins, and renal naturiesis (Hirata et al., 1993). The ET_A:ET_B ratio explains why ET-1 acts as a vasoconstrictor in some vascular beds and a vasodilator systemically. Of note, mice with deletions of one copy of Edn1 ($Edn1^{+/-}$) display hypertension, a result consistent with our working model (Kurihara et al., 1994). Additionally, ET-1 can reduce blood pressure by promoting diuresis and natriuresis via ET_B receptors in the renal collecting system (Ge et al., 2005; Kohan et al., 2011). In Figure 7, we summarize the multiple physiologic effects of ET-1 on the vasculature, and we propose a hypothetical model for the relationship between the G allele at rs9349379 and risk for five vascular diseases.

One challenge with the functional assessment of common, non-coding variation is the modest effect each variant has on gene expression. In this study, the *cis*-regulatory effect of the causal variant is a 20% increase in *EDN1* expression in the genome-edited ECs homozygous for the G allele. These data are consistent with several examples of non-coding, common variation with this modest level of transcriptional regulation (Bauer et al., 2013; Musunuru et al., 2010; Smemo et al., 2014; Sur et al., 2012; Tewhey et al., 2016). In each case, the effect of a common variant on gene expression is modest; however, stronger perturbation of the causal gene by either genetic (e.g., gene deletion) or pharmacologic means can lead to larger effects.

A second challenge in the study of non-coding variation is understanding the mechanism of distal regulation. Though, in the majority of cases, variants regulate the most proximal gene (Shin et al., 2014), long-range chromatin interactions can mediate distal regulatory effects. Newly available methods to characterize the regulatory elements and 3D architecture in GWAS loci allow a broader assessment of relevant genes. Here we demonstrate the regulation of a gene 600 kb from the causal variant. The mechanism of the distal *cis*-regulatory effect at 6q24 does not appear to be through canonical enhancer-promoter contact. Instead, the data point to a common contact site approximately 300 kb from both the *EDN1* promoter and rs9349379 regulatory element. This common contact site also contains a series of strong enhancers, as demonstrated by H3K27Ac signal. Recent studies support the notion that enhancer regulation of gene expression may include mechanisms that do not involve direct contact with a promoter. Enhancers can affect transcription through

interactions with insulators (Flavahan et al., 2016), promoters for distal genes (Fukaya et al., 2016), and other enhancers (Vockley et al., 2016). The *EDN1* locus may represent another example of such distal regulation, but further work is necessary to establish the mechanism by which the common contact site mediates gene expression.

In summary, we provide several lines of evidence that a common DNA variant associated with five vascular diseases regulates a gene, *EDN1*, located over 600 kb upstream in genomic distance. Selective modulation of endothelin-1 function in the appropriate vascular bed may prove useful in the treatment of diseases, such as CAD, migraine headache, cervical artery dissection, fibromuscular dysplasia, and hypertension.

Detailed methods are provided in the online version of this paper and include the following:

Contact for Reagent and Resource Sharing

Further information and requests for resources and reagents should be directed to and will be fulfilled by the Lead Contact, Rajat Gupta (rgupta@broadinstitute.org).

MTAs are required for human pluripotent stem cell lines. MTAs can be obtained through the Harvard Stem Cell Institute iPSC Core.

Experimental Model and Subject Details

Cell Lines

Pluripotent stem cell lines—All pluripotent stem cell lines are grown in mTeSR1 media, and supplemented with Y-27632 at passaging. Standard culture conditions (37°C, 5% CO_2). Human embryonic stem cell lines HUES 9 and HUES 66 and induced pluripotent stem cell line 1016 were obtained from the Harvard Stem Cell Institute after completion of a material transfer agreement. Cells were authenticated and karyotyped at the time of purchase.

DiPS 1016SevA iPSC cells: Reprogrammed from Fibroblasts by Sendai Virus method. Healthy male donor.

HUES 9: Hematopoetic stem cell, Female donor

HUES66: Hematopoetic stem cell, Female donor.

Primary Cell Cultures—All primary human endothelial cell lines were purchased from Lifeline Cell Technology, and grown in VascuLife EC Growth Media using standard culture conditions (37°C, 5% CO_2). Human coronary artery endothelial cells were from a deceased female donor, and human aortic endothelial cells were from a deceased male donor.

Primary human monocytes—Primary human CD14+ monocytes were isolated from peripheral blood (Leukopacs, MGH blood bank) by positive selection using CD14 MicroBeads (Miltenyi) according to the manufacturer's instructions. Three samples were obtained, representing 2 male and 1 female donors.

Human subjects—De-identified plasma samples were obtained from the Partners Healthcare Biobank. All participants are consented upon enrollment in the Biobank, and separate IRB approval is not required for these de-identified samples. Samples were selected for participant age 20-49 years, no current smoking, no hypertension diagnosis or anti-hypertensive use, no other medical diagnoses (defined by Charlson comorbidity index of 1), caucasian race. 99 plasma samples were obtained, 33 of each genotype at rs9349379 (A/A, A/G, G/G). 72 samples were from female donors, 28 from male donors with an even distribution of male and female samples in each genotype group.

Method Details

Association analyses in population cohorts

Phenome-wide association analysis in UK Biobank—We conducted a PheWAS for this variant in the UK Biobank (http://www.ukbiobank.ac.uk) using individual-level data from 112,338 individuals of European ancestry. Presence of 36 different diseases at baseline were defined by verbal interview with a trained nurse (definitions are provided in Table S2). Logistic regression, adjusting for age, sex, ten principal components of ancestry and a dummy variable for the array type used in genotyping, was used to test for the presence of association between rs9349379 and each of the 36 different diseases. A Bonferroni-adjusted p value of 0.0014 (0.05/36) was used as the threshold for statistical significance.

Arterial Stiffness Index Analysis

In UK Biobank, 38,795 individuals of European ancestry with available genotype data and arterial stiffness index (ASI) measurement were analyzed. ASI was measured by the PulseTrace PCA2 device (CareFusion, San Diego, USA). The PulseTrace PCA2 device is a pulse-wave, infra-red sensor that is placed on the participant's digit. ASI is defined as the participant's height divided by the time from when an initial pulse wave reaches the digital tip to when the same pulse wave travels through the aorta and lower extremity arterial system, and reflects back to the digital sensor. As such, larger ASI values reflect stiffer large arterial circulation. Extreme outliers (5 > standard deviations from the mean) were excluded. Association analysis in UK Biobank consisted of linear regression, ASI as the dependent variable, SNPs coded in an additive model, and covariates of age, sex, array type, and principal components utilizing R and PLINK (http://zzz.bwh.harvard.edu/plink/) statistical software programs.

Flow-mediated vasodilation Analysis

Flow-mediated vasodilation was assessed by ultrasound measurement of brachial artery diameter before and after sphygmomano-metric cuff inflation measured in 16,662 individuals from 6 cohorts of the Cohorts for Heart and Aging Research in Genomic Epidemiology (CHARGE) consortium: Cardiovascular Health Study (CHS, N = 1,697), Framingham Heart Study (FHS, N = 6388), Gutenberg Health Study (GHS, N = 3,975), Prospective Investigation of the Vasculature in Uppsala Seniors (PIVUS, N = 926), Study of Health in Pomerania (SHIP, N = 1,278), and Young Finns Study (YFS, N = 2,398). Genotyping was performed using Illumina 370 CNV BeadChip in CHS, Affymetrix Human Mapping 500K Array Set and 50K Human Gene Focused Panel in FHS, Affymetrix Whole-

Genome Human SNP Array 6.0 in GHS and SHIP, Illumina HumanHap 670k in YFS and Illumina Infinium Omni Express in the PIVUS study. Associations of rs9349379 on flow-mediated dilation were calculated separately in each study by linear regression under the assumption of an additive genetic model and adjusted for age and gender. Results from the individual cohorts were pooled using fixed-effects meta-analysis with inverse-variance weighting.

ENCODE analysis

Histone marks in the 6p24 locus were queried from the Roadmap epigenomics database. Analysis was conducted across all available tissue types in ENCODE phase one and two data. Newly released ENCODE phase 3 includes four aorta samples.

Re-analyzed, publicly available data:

ChIP-Seq in aortic tissue—Histone modification ChIP-seq data can be accessed via the ENCODE project data portal.

Separate links for the 4 Aortic tissue samples are:

https://www.encodeproject.org/experiments/ENCSR015GFK/

https://www.encodeproject.org/experiments/ENCSR318HUC/

https://www.encodeproject.org/experiments/ENCSR069UMW/

https://www.encodeproject.org/experiments/ENCSR982QIF/

Analysis of histone marks was conducted using coordinates chr6:12,850,000-12,960,000. Rpm/bp plots were generated for H3K27Ac, H3K4me3, H3K36me3, H3K27me3, H3K9me3 using bamplot software (Lin Lab: https://github.com/linlabbcm/bamplot).

4C-Sequencing Analysis

4C-seq was performed as previously described (van de Werken et al., 2012) using DpnII for the first digestion, and Csp6I for the second digestion. In brief, cells were crosslinked in 2% formaldehyde-PBS-10% FCS for 10 min at room temperature. After crosslinking, cells were incubated in lysis buffer while tumbling for an hour at 4°C. Cells were pelleted, washed, and resuspended in DpnII buffer. SDS was added to a concentration of 0.3% for an hour incubation in a thermomixer at 37°C and 400 rpm. Triton X-100 was then added to a concentration of 2.6% and cells were incubated for another hour. 200 units of DpnII enzyme were added for a 4 hr incubation in a thermomixer at 37°C and 900 rpm; another 200 units of DpnII were added for overnight incubation. Cells were then incubated for 20 min at 65°C to heat inactivate DpnII, suspended with ligation buffer and 50 units of ligase to a volume of 7 mL and then incubated overnight at 16°C. 300 μg Proteinase K was added for overnight incubation at 65°C. DNA was purified using NucleoMag P-Beads and taken up in restriction buffer with 50 units of Csp6I and incubated for 4 hr in a thermomixer at 37°C and 900 rpm, followed by heat inactivation of the enzyme (65° for 25 min). Sample was diluted with ligation buffer to a DNA concentration of <5 ng/μl. 100 units of ligase was then added for

overnight incubation at 16°C. DNA was purified using NucleoMag P-Beads and taken up in 5mM Tris pH7.5.

The 4C-seq PCRs were performed using rs9349379 (reading primer TTATCCTTATTCATTTGATC and non-reading primer CTTTGCCCTTAGAAAGGTTT) and the EDN1 promoter (reading primer GGTTTGGACAGACTCAGATC and non-reading primer TGTCTAACCTGAAAAATGGG) as viewpoints. Primers were extended with dangling Illumina adaptor sequences. Viewpoint fragments were selected based on fragment size (DpnII-DpnII > 400 bp), fragment-end size (DpnII-Csp6I > 200 bp) and opportunities for specific primer design (Primer 3) close to (< 20 bp away from) the DpnII primary restriction site (van de Werken et al., 2012).

Sequencing reads were demultiplexed and trimmed of the primer sequence using demultiplex.py from FourCSeq package (Klein et al., 2015), aligned using bowtie2 (v2.2.5) with standard parameters and quality filter set to 1 (-q 1) and processed as described (van de Werken et al., 2012). In short, reads are mapped to a restricted human reference genome (hg19), consisting of sequences directly flanking the 4C primary restriction enzyme site (DpnII), called 4C frag-ends. Non-unique frag-ends are discarded in subsequent analysis. After mapping, the highest covered frag-end was removed from the dataset in the normalization process and data are read-depth normalized to 1 million aligned intrachromosomal reads. 4C-Seq coverage profiles are calculated as “running means,” i.e., coverage averages of 21 consecutive 4C frag-ends.

Luciferase expression constructs

To functionally validate the common contact region, 2kB segments surrounding each H3K27Ac peak were cloned into the multiple cloning site of the pGL4-SV40 vector (Promega) using standard restriction-enzyme cloning or Gibson assembly. All constructs were verified by Sanger sequencing of plasmids.

Luciferase reporter assays

293T cells were routinely cultured in DMEM/10% FBS until ready for transfection. Bovine aortic endothelial cells (Cell Applications) were routinely cultured in DMEM/10% FBS until ready for transfection. 10,000 293T cells or 20,000 bovine aortic endothelial cells were plated in each well of a 96-well plate and transfected with 100ng of total plasmid DNA. Luciferase plasmids were co-transfected with renilla plasmids as a transfection control in either a 1:1 ratio (293T cells) or 1:5 ratio (bovine aortic endothelial cells). 293T cells were transfected using FuGene 6 (Promega) and bovine aortic endothelial cells were transfected using Viafect (Promega). Twenty-four hours after transfection, firefly and renilla luciferase activities were measured using the Dual-Luciferase Reporter Assay System (Promega) according to the manufacturer's protocol.

CRISPR/Cas9 guide selection and cloning

Using computational algorithms with prioritization for on-target efficiency and reduced off-target effects (available online: CRISPR Design tool (crispr.mit.edu), we identified Streptococcus pyogenes Cas9 (SpCas9) guide RNAs that bind near rs9349379. We selected

all possible sgRNA sequences within 100bp of the target SNP (rs9349379). Annealed oligomers inclusive of guide RNA sequences were subcloned into the PX459v2 plasmid, which contains expression cassettes for the guide RNA, a human codon-optimized Cas9, a puromycin resistance gene. Plasmids were transformed into chemically competent *E. coli* (Sbtl3, Thermofisher), and grown; plasmid DNA was extracted and purified.

Surveyor assays

293T cells were routinely grown in DMEM/10% FBS until ready for transfection. 40,000 293T cells were transfected with 1ug of each CRISPR construct. Genomic DNA was harvested and a 280 base pair region flanking rs9349379 was PCR-amplified and purified. Purified product was heteroduplexed, digested with Surveyor nuclease, and products run on a 2% agarose gel. Cleavage patterns were qualitatively analyzed to determine constructs cutting efficiency to guide further experiments.

Genome editing in human stem cells

Human embryonic and induced pluripotent stem cell lines were genotyped at rs9349379 via Sanger sequencing. Cells were routinely grown in mTeSR1 media, with Y-27632 at passaging, until ready for transfection. 800,000 stem cells were nucleofected with 5ug of CRISPR plasmid constructs and 7.5ug of a 200bp single single-stranded oligodeoxynucleotide donor template (ssODN). Following transfection, stem cells underwent 48 hr of puromycin selection at 1ug/mL (Hues 9 and 1016) or 0.5ug/mL (Hues 66). Following 5 days of cell growth, individual colonies were isolated, genomic DNA was extracted and PCR amplified, and screened for desired mutations. To account for off-target effects of the Cas9 nuclease, 3 wild-type and 3 clones with each desired mutations were expanded.

To delete 88 base pairs of noncoding sequence around rs9349379, we utilized a dual-guide RNA strategy using two Cas9-guide RNA constructs with 80bp of spacing between guide RNAs. These deletions were generated in both a homozygous major induced pluripotent stem cell line (1016) and a homozygous minor embryonic stem cell line (Hues 9). Genomic deletions were screened for with agarose gel electrophoresis of PCR amplicons and confirmed with Sanger sequencing of PCR amplicons. In each cell line, 3 wild-type and 3 biallelic 88 base pair deletions were selected for further study.

Due to the nature of non-coding sequence, minimal SpCas9 protospacer adjacent motifs (PAMs), which are required for Cas9-guide RNA recognition of target sequence, were available for genome editing at rs9349379. Hence, we pursued two rounds of genome editing to introduce a single base pair variant. The first round of editing replaced rs9349379 and the two adjacent base pairs with guanine nucleotides. Individual colonies with replaced nucleotides were expanded for the second round of genome editing, utilizing the new guanine nucleotides as PAMs. To restore wild-type sequence and insert a single variant at rs9349379, ssODNs containing either the major or minor allele (wild-type elsewhere) were used as repair templates. 3 homozygous major and 3 homozygous minor clones were selected for further study.

sgRNA sequences

sgRNA	Sequence	PAM
5′ Δ88 Guide1	TTAAGAAGCATGAGTAAAA	TGG
3′ Δ88 Guide 2	CGTGGAAAATATAACTA	TGG
Precise editing, round 1	CGTGGAAAATATAACTA	TGG
Precise editing, round 2-A	TGCCCTTGAGATCATATAA	AGG
Precise editing, round 2-B	GCCCTTGAGATCATATAAA	GGG
Precise editing, round 2-C	TAGCCAATGATTTTAAGCT	GGG
Precise editing, round 2-D	ATAGCCAATGATTTTAAGC	TGG

ssODN sequences

ssODN - GGG at rs9349379	ATAACTCAGTACATAATCATTAAGAAGCATGAG TAAAATGGGATTTTAATTACTTTATTAAAGGTAAT AAATATGTCTATGCCCTTGAGATCATAT AAAGGGAGCTTAAAATCATTGGCTATAGTTATA TTTTCCACGAGCTGAGTTTTAAAATATGTATAAA GTCTGTGGTAAATTAAGAGAGATTTCAG CCTACTAAC
ssODN - CCC at rs9349379	ATAACTCAGTACATAATCATTAAGAAGCATGA GTAAAATGGGATTTTAATTACTTTATTAAAGG TAATAAATATGTCTATGCCCTTGAGATCATATA AACCCAGCTTAAAATCATTGGCTATAGTTATATT TTCCACGAGCTGAGTTTTAAAATATGTATAAAG TCTGTGGTAAATTAAGAGAGATTTCAGCC TACTAAC
ssODN - A	ATAACTCAGTACATAATCATTAAGAAGCATGAG TAAAATGGGATTTTAATTACTTTATTAAAGGTA ATAAATATGTCTATGCCCTTGAGATCATATA AAAATAGCTTAAAATCATTGGCCATAGTTATA TTTTCCACGAGCTGAGTTTTAAAATATGTATAAA GTCTGTGGTAAATTAAGAGAGATTTCAGCC TACTAAC
ssODN - G	ATAACTCAGTACATAATCATTAAGAAGCATGAG TAAAATGGGATTTTAATTACTTTATTAAAGGTAAT AAATATGTCTATGCCCTTGAGATCATATA AAAGTAGCTTAAAATCATTGGCCATAGTTATATT TTCCACGAGCTGAGTTTTAAAATATGTATAAA GTCTGTGGTAAATTAAGAGAGATTTCAGCC TACTAAC

Cpf1 sequences

Species	Construct	Guide
Acidaminococcus	CR1	TATATGATCTCAAGGGCATAGAC
Acidaminococcus	CR2	AGCTATTTTTATATGATCTCAAG
Acidaminococcus	CR3	AGCTACTTTTATATGATCTCAAG
Acidaminococcus	CR4	TTATATGATCTCAAGGGCATAGA

Lachnospiraceae	CR1	TATATGATCTCAAGGGCATAGAC
Lachnospiraceae	CR2	AGCTATTTTTATATGATCTCAAG
Lachnospiraceae	CR3	AGCTACTTTTATATGATCTCAAG
Lachnospiraceae	CR4	TTATATGATCTCAAGGGCATAGA

Stem cell differentiation

All cell cultures were routinely passaged using Accutase (StemCell Technologies) and maintained on Geltrex LDEV-Free Reduced Growth Factor Basement Membrane Matrix (ThermoFisher Scientific) coated dishes in mTeSR1 (Stem Cell Technologies).

For Endothelial Cell (EC) differentiation, cell lines were plated on Geltrex Basement Membrane Matrix coated dishes in mTeSR1 with 10 μM ROCK inhibitor Y-27632 (Calbiochem) at a density of 27,000-28,000 cells/cm^2. After 24 hr, culture was replaced with Priming Medium, consisting N2B27 medium [1:1 mixture of DMEM/F12 and Neurobasal media supplemented with N2 and B27 (Invitrogen) and β-Mercaptoethanol (Sigma-Aldrich)] with 6μM CHIR-99021 (Cayman Chemical) and 25 ng/ml BMP4 (R&D Systems). After three days, priming medium was replaced by EC Induction Medium consisting of StemPro-34 SFM medium (Invitrogen) supplemented with 200ng/ml VEGF (PeproTech) and 2 μM Forskolin (Sigma-Aldrich). The Induction Medium was renewed after one day. On day six, the differentiated ECs were dissociated with Accutase and manually separated using CD144 MicroBeads (Miltenyi Biotec). CD144-positive cells were replated on dishes at a density of 25,000 cells/cm^2 in VascuLife VEGF Endothelial Medium (Lifeline Cell Tech). The VEGF Endothelial Medium was renewed every three days.

Neural Crest Cells (NCC) were generated from human induced Pluripotent Stem Cells (hiPSCs) using a LSB-short dual SMAD inhibition pathway (Kreitzer et al., 2013). Human induced Pluripotent Stem Cells (hiPSCs) were maintained on Geltrex-coated (ThermoFisher Scientific) tissue culture dishes in mTesR1 (STEMCELL Technologies). To initiate the neural priming step, hiPSCs were plated at a density of 104 cells/cm2 on Geltrex-coated (ThermoFisher Scientific) 6-well plates in N2B27-CDM media supplemented with 20ng/mL bFGF (R&D Systems) and 10uM Y-27632 (Santa Cruz Biotech). For the next three days, N2B27-CDM was replaced with medium lacking Y-27632 (Santa Cruz Biotech). To promote neural induction, cells were incubated with varying ratios of KSR:N2 media on day 4 (100:0), day 5 (75:25), day 6 (50:50), day 7 (25:75), and day 8 (0:100), and supplemented with 50nM LDN-13189 (Stemgent) and 5uM SB431542 (Tocris). Total RNA of biological triplicates was extracted using TRIzol reagent (Life Technologies) and purified for gene expression analysis.

Gene expression analysis

Sorted vascular endothelial cells were plated at approximately 65,000 cells/cm^2 and allowed to grow for 2 days. RNA was harvested using TRIzol reagent and purified. 1ug of RNA was reverse transcribed into cDNA. RNA-sequencing was conducted on samples with RIN of 10 (Agilent Technologies). Samples were prepared for sequencing with SMART-Seq2 protocol

and Illumina barcodes. Sequencing performed on Illumina NextSeq500 using High Ouput v2 kit to generate 2 × 25bp reads. Computation analysis of paired-end reads was conducted using Kallisto/Sleuth software package (Bray et al., 2016). Sample plots and differential expression conducted using R software. Gene-set enrichment analysis conducted using clusterprofiler R software package.

Confirmatory qPCR conducted on EDN1, *PHACTR1*, SIRT1, GFOD1, HIVEP1, and TBC1D7 was assessed using validated probes, with HPRT1 as a reference gene. Gene expression was assayed on Bio-Rad CFX384 real-time PCR detection system. Probes used were Hs01116214_m1 (PHACTR1, exons 12-13), Hs00174961_m1 (EDN1), Hs00212898_m1 (TBC1D7), Hs00978335_m1 (SIRT5), Hs00172428_m1 (HIVEP1), Hs00255879_m1 (GFOD1), and control VIC Human HPRT1 (43108980E) all from Life Technologies.

After serum starvation, cells were either stimulated with 50ng/mL IL1alpha (PeproTech) or treated with 0.5% FCS in VEGF Endothelial Basal Medium as a control. After 3 hr stimulation, RNA was harvested using TRIzol reagent and purified for gene expression analysis.

Big ET-1 ELISA

CD144-positive cells were seeded on 12 well plates at a cell density of 70,000 cells/cm^2 in VascuLife VEGF Endothelial Medium. Next day, culture was serum starved with 0.5% FCS in VEGF Endothelial Basal Medium for 6 hr. After serum starvation, cells were either stimulated with 50ng/mL IL1alpha (PeproTech) or treated with 0.5% FCS in VEGF Endothelial Basal Medium as a control. At 24 hr stimulation, supernatant was harvested for Big-ET1 ELISA analysis (Enzo Life Sciences). Assay was performed according to manufacturer instructions. Briefly, cell-free supernatant was incubated overnight at 4°C on microtiter plate with immobilized anti-Big ET-1 polyclonal antibody. Plate is washed 7 times, and incubated with secondary rabbit polyclonal antibody to Big ET-1 labeled with Horseradish peroxidase. Plate is again washed 7 times, incubated with substrate, and read at 450nm on a microplate reader. Sensitivity of assay (according to manufacturer) is 0.23 pg/mL (range 0.78-100pg/mL). Cells were simultaneously lysed in Cell Lysis Buffer supplemented with PMSF (Cell Signaling) and assayed for total protein by BCA (Thermo). Results are represented as Big ET-1 levels divided by total protein.

Chromatin immunoprecipitation-sequencing (ChIP-seq)

For histone modification ChIP-Seq, 7 million iPSC-ECs cells were cross-linked in growth media +1% formaldehyde for 10 min at 37°C, quenched for 5 min with 125 mmol/L glycine, washed twice in cold PBS with protease inhibitors, and stored at −80°C. ChIP and sequencing library preparation were performed by standard methods. Cross-linked cell line pellets were thawed and lysed in cold cytoplasmic lysis buffer (20 mM Tris-HCl ph8.0, 85 mM KCl, 0.5% IGEPAL CA-630 + PI). Nuclei were pelleted at 3000 g, re-suspended in cold SDS lysis buffer (1% SDS, 10mM EDTA, 50mM Tris-HCl, pH 8.1 + PI) for 10 min, and sonicated to an average fragment size of 200-400 bp on a Branson sonifier. Sonication settings were as follows: 0.7 son, 1.3 s off for 5-8 min of total sonication time, amplitude

~45%, adjusted as needed for a power output of 10-12 W. Samples were diluted 1:10 in ChIP dilution buffer (0.01% SDS, 0.25% Triton X-100, 1.2mM EDTA, 16.7mM Tris-HCl, pH 8.1, 167mM NaCl +PI), and rotated at 4°C overnight with 2-5 ug of antibody. Antibody used was H3K27ac (39133, Active Motif). Antigen-antibody complexes were collected with protein G Dynabeads (Life technologies) for 4 hr at 4°C, and sequentially washed 2-6× each with RIPA buffer (0.1% sodium deoxycholate, 0.1% SDS, 1% Triton x-100, 10mM Tris-HCl pH 8.0, 1mM EDTA, 140 Mm NaCl), RIPA/high salt buffer (0.1% DOC, 0.1% SDS, 1% Triton x-100, 10mM Tris-HCl pH 8.0, 1mM EDTA, 360 mM NaCl), LiCl wash buffer (250mM LiCl, 0.5% NP40, 0.5% deoxycholate, 1mM EDTA, 10mM Tris-HCl, pH 8.0), and TE Buffer pH 8.0 (10mM Tris-HCl pH 8.0, 1mM EDTA). Beads were then resuspended in Low-SDS ChIPelution buffer (10mM Tris-HCl pH 8.0, 0.5M EDTA, 300mM NaCl, 0.1% SDS, 5mM DTT) and incubated for 6 hr at 65°C to elute DNA and reverse crosslinking. Supernatants were treated with RNase and proteinase K, and ChIP DNA was then purified with AMPure beads (Beckman-Coulter). For sequencing library preparation, ChIP DNA was end-repaired (End-It, Epicenter), A-tailed (Kle-now fragment 3′→5′ exo-, New England Biolabs), and ligated to barcoded illumina adaptors (Quick T4 DNA ligase, NEB). Each reaction was followed by clean-up with AMPure beads. Ligation products were amplified by PCR for 14-18 cycles with illumina indexing primers and PFU Ultra II HS PCR mix (Agilent). Library size selection to 300-600 bp was performed by gel purification (E-Gel SizeSelect 2%, Life technologies) or two-step AMPure bead selection. Paired-end sequencing of H3K27ac ChIP libraries was performed on a HiSeq 2500 or NextSeq, with read lengths of 36 bp + 25 bp or 38 bp + 38 bp. ChIP-seq tracks were generated and visualized with the Integrative Genomics Viewer (IGV). Super-enhancer analysis of H3K27ac ChIP-seq was performed with MACS and ROSE computation packages. ChIP datasets are available through the ENCODE website (https://www.encodeproject.org). Publicly available ChIP-seq data were used to confirm findings from iPSC-ECs. (HUVEC, H3K27Ac ChIP-seq: GEO Data GSE53998; (Brown et al., 2014) iPSC/Embryonic-EC, H3K27Ac ChIP-seq: (GNomEx, Accession number: 195R2; (Theodoris et al., 2015)).

Big ET-1 measurement in human plasma samples

Human plasma samples obtained from Partners Healthcare biobank of de-identified patient samples. 33 samples of each genotype at rs9349379 were selected. Samples were limited to those with Charlson Comorbidity Scores of 0, and individuals not taking any antihypertensive medications. Big ET-1 was measured by ELISA (Enzo Life Sciences) as described above.

Quantification and Statistical Analysis

Phenotypic associations were analyzed using logistic regression, adjusting for age, sex, ten principal components of ancestry and a dummy variable for the array type used in genotyping, was used to test for the presence of association between rs9349379 and each of the 36 different diseases. A Bonferroni-adjusted p value of 0.0014 (0.05/36) was used as the threshold for statistical significance.

Real-time PCR analysis was conducted on cDNA samples generated from stem cell-derived cells (endothelial cells, vascular smooth muscle cells, neural crest progenitor cells). All experiments used 3 separately differentiated cellular clones, and differentiation was conducted in parallel. Data represent the average of three technical replicates per clone, and statistical analysis on three independently differentiated clones (n = 3). Statistical analysis and plot generation conducted using Graphpad Prism software (www.graphpad.com). Statistical analysis performed using parametric Student's t test.

ELISA quantification performed on cell-free supernatants from cultured endothelial cells. Each experiment included 9 samples (3 independently differentiated clones, cultured in 3 wells each). Absorbance values from ELISA were converted to pg/mL using a standard curve. Total protein from extracted cells used to normalize values for each well in experiment. Results presented as Big ET-1 divided by Total Protein ratio. Statistical analysis performed using parametric Student's t test.

RNA sequencing was conducted on cDNA samples from stem cell-derived endothelial cells. 3 homozygous major (A/A) and 3 homozygous minor (G/G) stem cell lines were differentiated into ECs as described above. Count data were collapsed to gene level analysis by ENSEMBL gene name. Statistical analysis performed using Wald test using the SLEUTH software package in R (http://pachterlab.github.io/sleuth/about).

Human plasma BigET-1 levels were analyzed using additive model of linear regression with sex and age as co-variates. Software used for all statistical analysis was R software package (https://r-project.org).

Data and Software Availability

RNaseq data posted on Mendeley

FASTQ files for AA1, AA2: http://dx.doi.org/10.17632/z259mb2tvy.1

FASTQ files for AA3, GG1: http://dx.doi.org/10.17632/9frfyyhdc2.1

FASTQ files for GG2, GG3: http://dx.doi.org/10.17632/9hccrsn9s3.1; http://dx.doi.org/10.17632/xhhvsm9r5k.1

ChIP-Seq in iPSC-ECs posted on Mendeley

BAM files: http://dx.doi.org/10.17632/jznmppxyrd.1

Supplementary Material

Refer to Web version on PubMed Central for supplementary material.

Acknowledgments

This work was supported by a Sarnoff Scholar Award, a Harvard Catalyst CMERIT Award, and NIH NHLBI K08-HL128810 (to R.M.G.); NIH T32 HL007734 (to D.K.); NIH NHGRI U54HG006991 to B.E.B.; and NIH NIDDK R01 DK097768, Fondation Leducq CVGeneF(x) Transatlantic Network of Excellence, NIH R01HL127564, and the Ofer and Shelly Nemirovsky MGH Research Scholar Award (to S.K.). The CHARGE endothelial function working group provided data for FMD analysis. S.K. reports receiving grants from Bayer Healthcare, Amarin, and Regeneron; serving on scientific advisory boards for Catabasis, Regeneron Genetics Center, Merck, Celera, and

Genomics PLC; receiving consulting fees from Novartis, Sanofi, AstraZeneca, Alnylam, Eli Lilly, Lerink Partners, Noble Insights, Merck, Quest Diagnostics, Amgen, Genentech, Corvidia, Ionis Pharmaceuticals, and Eli Lilly; and holding equity in Catabasis and San Therapeutics.

References

Aguet, F., Brown, AA., Castel, S., Davis, JR., Mohammadi, P., Segre, AV., Zappala, Z., Abell, NS., Fresard, L., Gamazon, ER., et al. Local genetic effects on gene expression across 44 human tissues. bioRxiv. 2016. http://dx.doi.org/10.1101/074450

Amiri F, Virdis A, Neves MF, Iglarz M, Seidah NG, Touyz RM, Reudelhuber TL, Schiffrin EL. Endothelium-restricted overexpression of human endothelin-1 causes vascular remodeling and endothelial dysfunction. Circulation. 2004; 110:2233–2240. [PubMed: 15466627]

Anttila V, Winsvold BS, Gormley P, Kurth T, Bettella F, McMahon G, Kallela M, Malik R, de Vries B, Terwindt G, et al. North American Brain Expression Consortium; UK Brain Expression Consortium; International Headache Genetics Consortium. Genome-wide meta-analysis identifies new susceptibility loci for migraine. Nat Genet. 2013; 45:912–917. [PubMed: 23793025]

Asghar MS, Hansen AE, Amin FM, van der Geest RJ, Koning Pv, Larsson HBW, Olesen J, Ashina M. Evidence for a vascular factor in migraine. Ann Neurol. 2011; 69:635–645. [PubMed: 21416486]

Bacon CR, Cary NRB, Davenport AP. Endothelin peptide and receptors in human atherosclerotic coronary artery and aorta. Circ Res. 1996; 79:794–801. [PubMed: 8831503]

Barton M, Haudenschild CC, d'Uscio LV, Shaw S, Münter K, Lüscher TF. Endothelin ETA receptor blockade restores NO-mediated endothelial function and inhibits atherosclerosis in apolipoprotein E-deficient mice. Proc Natl Acad Sci USA. 1998; 95:14367–14372. [PubMed: 9826706]

Bauer DE, Kamran SC, Lessard S, Xu J, Fujiwara Y, Lin C, Shao Z, Canver MC, Smith EC, Pinello L, et al. An erythroid enhancer of BCL11A subject to genetic variation determines fetal hemoglobin level. Science. 2013; 342:253–257. [PubMed: 24115442]

Bauer RC, Tohyama J, Cui J, Cheng L, Yang J, Zhang X, Ou K, Paschos GK, Zheng XL, Parmacek MS, et al. Knockout of Adamts7, a novel coronary artery disease locus in humans, reduces atherosclerosis in mice. Circulation. 2015; 131:1202–1213. [PubMed: 25712206]

Beaudoin M, Gupta RM, Won HH, Lo KS, Do R, Henderson CA, Lavoie-St-Amour C, Langlois S, Rivas D, Lehoux S, et al. Myocardial Infarction-Associated SNP at 6p24 Interferes With MEF2 Binding and Associates With PHACTR1 Expression Levels in Human Coronary Arteries. Arterioscler Thromb Vasc Biol. 2015; 35:1472–1479. [PubMed: 25838425]

Bolay H, Reuter U, Dunn AK, Huang Z, Boas DA, Moskowitz MA. Intrinsic brain activity triggers trigeminal meningeal afferents in a migraine model. Nat Med. 2002; 8:136–142. [PubMed: 11821897]

Brown JD, Lin CY, Duan Q, Griffin G, Federation AJ, Paranal RM, Bair S, Newton G, Lichtman AH, Kung AL, et al. NF-κB directs dynamic super enhancer formation in inflammation and atherogenesis. Mol Cell. 2014; 56:219–231. [PubMed: 25263595]

Bray NL, Pimentel H, Melsted P, Pachter L. Near-optimal probabilistic RNA-seq quantification. Nat Biotechnol. 2016; 34:525–527. [PubMed: 27043002]

Deloukas P, Kanoni S, Willenborg C, Farrall M, Assimes TL, Thompson JR, Ingelsson E, Saleheen D, Erdmann J, Goldstein BA, et al. CARDIoGRAMplusC4D Consortium. Large-scale association analysis identifies new risk loci for coronary artery disease. Nat Genet. 2013; 45:25–33. [PubMed: 23202125]

Corretti MC, Anderson TJ, Benjamin EJ, Celermajer D, Charbonneau F, Creager MA, Deanfield J, Drexler H, Gerhard-Herman M, Herrington D, et al. International Brachial Artery Reactivity Task Force. Guidelines for the ultrasound assessment of endothelial-dependent flow-mediated vasodilation of the brachial artery: a report of the International Brachial Artery Reactivity Task Force. J Am Coll Cardiol. 2002; 39:257–265. [PubMed: 11788217]

Debette S, Kamatani Y, Metso TM, Kloss M, Chauhan G, Engelter ST, Pezzini A, Thijs V, Markus HS, Dichgans M, et al. International Stroke Genetics Consortium; CADISP Group. Common variation in PHACTR1 is associated with susceptibility to cervical artery dissection. Nat Genet. 2015; 47:78–83. [PubMed: 25420145]

Deng W, Lee J, Wang H, Miller J, Reik A, Gregory PD, Dean A, Blobel GA. Controlling long-range genomic interactions at a native locus by targeted tethering of a looping factor. Cell. 2012; 149:1233–1244. [PubMed: 22682246]

Dowen JM, Fan ZP, Hnisz D, Ren G, Abraham BJ, Zhang LN, Wein-traub AS, Schuijers J, Lee TI, Zhao K, Young RA. Control of cell identity genes occurs in insulated neighborhoods in mammalian chromosomes. Cell. 2014; 159:374–387. [PubMed: 25303531]

ENCODE Project Consortium. An integrated encyclopedia of DNA elements in the human genome. Nature. 2012; 489:57–74. [PubMed: 22955616]

Farh KKH, Marson A, Zhu J, Kleinewietfeld M, Housley WJ, Beik S, Shoresh N, Whitton H, Ryan RJH, Shishkin AA, et al. Genetic and epigenetic fine mapping of causal autoimmune disease variants. Nature. 2015; 518:337–343. [PubMed: 25363779]

Flavahan WA, Drier Y, Liau BB, Gillespie SM, Venteicher AS, Stemmer-Rachamimov AO, Suvà ML, Bernstein BE. Insulator dysfunction and oncogene activation in IDH mutant gliomas. Nature. 2016; 529:110–114. [PubMed: 26700815]

Fukaya T, Lim B, Levine M. Enhancer Control of Transcriptional Bursting. Cell. 2016; 166:358–368. [PubMed: 27293191]

Ge Y, Ahn D, Stricklett PK, Hughes AK, Yanagisawa M, Verbalis JG, Kohan DE. Collecting duct-specific knockout of endothelin-1 alters vasopressin regulation of urine osmolality. Am J Physiol Renal Physiol. 2005; 288:F912–F920. [PubMed: 15632412]

GTEx Consortium. The Genotype-Tissue Expression (GTEx) project. Nat Genet. 2013; 45:580–585. [PubMed: 23715323]

Hirata Y, Takagi Y, Fukuda Y, Marumo F. Endothelin is a potent mitogen for rat vascular smooth muscle cells. Atherosclerosis. 1989; 78:225–228. [PubMed: 2675859]

Hirata Y, Emori T, Eguchi S, Kanno K, Imai T, Ohta K, Marumo F. Endothelin receptor subtype B mediates synthesis of nitric oxide by cultured bovine endothelial cells. J Clin Invest. 1993; 91:1367–1373. [PubMed: 7682570]

Jarray R, Allain B, Borriello L, Biard D, Loukaci A, Larghero J, Hadj-Slimane R, Garbay C, Lepelletier Y, Raynaud F. Depletion of the novel protein PHACTR-1 from human endothelial cells abolishes tube formation and induces cell death receptor apoptosis. Biochimie. 2011; 93:1668–1675. [PubMed: 21798305]

Jarray R, Pavoni S, Borriello L, Allain B, Lopez N, Bianco S, Liu WQ, Biard D, Demange L, Hermine O, et al. Disruption of phactr-1 pathway triggers pro-inflammatory and pro-atherogenic factors: New insights in atherosclerosis development. Biochimie. 2015; 118:151–161. [PubMed: 26362351]

Kiando SR, Tucker NR, Castro-Vega LJ, Katz A, D'Escamard V, Tréard C, Fraher D, Albuisson J, Kadian-Dodov D, Ye Z, et al. PHACTR1 Is a Genetic Susceptibility Locus for Fibromuscular Dysplasia Supporting Its Complex Genetic Pattern of Inheritance. PLoS Genet. 2016; 12:e1006367. [PubMed: 27792790]

Klein FA, Pakozdi T, Anders S, Ghavi-Helm Y, Furlong EEM, Huber W. FourCSeq: analysis of 4C sequencing data. Bioinformatics. 2015; 31:3085–3091. [PubMed: 26034064]

Kohan DE, Rossi NF, Inscho EW, Pollock DM. Regulation of blood pressure and salt homeostasis by endothelin. Physiol Rev. 2011; 91:1–77. [PubMed: 21248162]

Kowala MC, Rose PM, Stein PD, Goller N, Recce R, Beyer S, Valentine M, Barton D, Durham SK. Selective blockade of the endothelin subtype A receptor decreases early atherosclerosis in hamsters fed cholesterol. Am J Pathol. 1995; 146:819–826. [PubMed: 7717449]

Kreitzer FR, Salomonis N, Sheehan A, Huang M, Park JS, Spindler MJ, Lizarraga P, Weiss WA, So PL, Conklin BR. A robust method to derive functional neural crest cells from human pluripotent stem cells. Am J Stem Cells. 2013; 2:119–131. [PubMed: 23862100]

Kurihara Y, Kurihara H, Suzuki H, Kodama T, Maemura K, Nagai R, Oda H, Kuwaki T, Cao WH, Kamada N, et al. Elevated blood pressure and craniofacial abnormalities in mice deficient in endothelin-1. Nature. 1994; 368:703–710. [PubMed: 8152482]

Li JS, Lariviére R, Schiffrin EL. Effect of a nonselective endo-thelin antagonist on vascular remodeling in deoxycorticosterone acetate-salt hypertensive rats. Evidence for a role of endothelin in vascular hypertrophy. Hypertension. 1994; 24:183–188. [PubMed: 8039842]

Li MW, Mian MOR, Barhoumi T, Rehman A, Mann K, Paradis P, Schiffrin EL. Endothelin-1 overexpression exacerbates atherosclerosis and induces aortic aneurysms in apolipoprotein E knockout mice. Arterioscler Thromb Vasc Biol. 2013; 33:2306–2315. [PubMed: 23887640]

Maruyama T, Dougan SK, Truttmann MC, Bilate AM, Ingram JR, Ploegh HL. Increasing the efficiency of precise genome editing with CRISPR-Cas9 by inhibition of nonhomologous end joining. Nat Biotechnol. 2015; 33:538–542. [PubMed: 25798939]

Maurano MT, Humbert R, Rynes E, Thurman RE, Haugen E, Wang H, Reynolds AP, Sandstrom R, Qu H, Brody J, et al. Systematic localization of common disease-associated variation in regulatory DNA. Science. 2012; 337:1190–1195. [PubMed: 22955828]

Musunuru K, Strong A, Frank-Kamenetsky M, Lee NE, Ahfeldt T, Sachs KV, Li X, Li H, Kuperwasser N, Ruda VM, et al. From noncoding variant to phenotype via SORT1 at the 1p13 cholesterol locus. Nature. 2010; 466:714–719. [PubMed: 20686566]

Stitziel NO, Stirrups KE, Masca NG, Erdmann J, Ferrario PG, König IR, Weeke PE, Webb TR, Auer PL, Schick UM, et al. Myocardial Infarction Genetics and CARDIoGRAM Exome Consortia Investigators. Coding Variation in ANGPTL4, LPL, and SVEP1 and the Risk of Coronary Disease. N Engl J Med. 2016; 374:1134–1144. [PubMed: 26934567]

Kathiresan S, Voight BF, Purcell S, Musunuru K, Ardissino D, Mannucci PM, Anand S, Engert JC, Samani NJ, Schunkert H, et al. Myocardial Infarction Genetics Consortium; Wellcome Trust Case Control Consortium. Genome-wide association of early-onset myocardial infarction with single nucleotide polymorphisms and copy number variants. Nat Genet. 2009; 41:334–341. [PubMed: 19198609]

Nikpay M, Goel A, Won HH, Hall LM, Willenborg C, Kanoni S, Saleheen D, Kyriakou T, Nelson CP, Hopewell JC, et al. CARDIoGRAMplusC4D Consortium. A comprehensive 1,000 Genomes-based genome-wide association meta-analysis of coronary artery disease. Nat Genet. 2015; 47:1121–1130. [PubMed: 26343387]

Nurnberg ST, Cheng K, Raiesdana A, Kundu R, Miller CL, Kim JB, Arora K, Carcamo-Oribe I, Xiong Y, Tellakula N, et al. Coronary Artery Disease Associated Transcription Factor TCF21 Regulates Smooth Muscle Precursor Cells That Contribute to the Fibrous Cap. PLoS Genet. 2015; 11:e1005155. [PubMed: 26020946]

O'Donnell CJ, Kavousi M, Smith AV, Kardia SLR, Feitosa MF, Hwang SJ, Sun YV, Province MA, Aspelund T, Dehghan A, et al. CARDIoGRAM Consortium. Genome-wide association study for coronary artery calcification with follow-up in myocardial infarction. Circulation. 2011; 124:2855–2864. [PubMed: 22144573]

Olin JW, Gornik HL, Bacharach JM, Biller J, Fine LJ, Gray BH, Gray WA, Gupta R, Hamburg NM, Katzen BT, et al. American Heart Association Council on Peripheral Vascular Disease; American Heart Association Council on Clinical Cardiology; American Heart Association Council on Cardiopulmonary, Critical Care, Perioperative and Resuscitation; American Heart Association Council on Cardiovascular Disease in the Young; American Heart Association Council on Cardiovascular Radiology and Intervention; American Heart Association Council on Epidemiology and Prevention; American Heart Association Council on Functional Genomics and Translational Biology; American Heart Association Council for High Blood Pressure Research; American Heart Association Council on the Kidney in Cardiovascular Disease; American Heart Association Stroke Council. Fibromuscular dysplasia: state of the science and critical unanswered questions: a scientific statement from the American Heart Association. Circulation. 2014; 129:1048–1078. [PubMed: 24548843]

Paquet D, Kwart D, Chen A, Sproul A, Jacob S, Teo S, Olsen KM, Gregg A, Noggle S, Tessier-Lavigne M. Efficient introduction of specific homozygous and heterozygous mutations using CRISPR/Cas9. Nature. 2016; 533:125–129. [PubMed: 27120160]

Parker SCJ, Stitzel ML, Taylor DL, Orozco JM, Erdos MR, Akiyama JA, van Bueren KL, Chines PS, Narisu N, Black BL, et al. NISC Comparative Sequencing Program; National Institutes of Health Intramural Sequencing Center Comparative Sequencing Program Authors; NISC Comparative Sequencing Program Authors. Chromatin stretch enhancer states drive cell-specific gene regulation and harbor human disease risk variants. Proc Natl Acad Sci USA. 2013; 110:17921–17926. [PubMed: 24127591]

Patsch C, Challet-Meylan L, Thoma EC, Urich E, Heckel T, O'Sullivan JF, Grainger SJ, Kapp FG, Sun L, Christensen K, et al. Generation of vascular endothelial and smooth muscle cells from human pluripotent stem cells. Nat Cell Biol. 2015; 17:994–1003. [PubMed: 26214132]

Peters DT, Cowan CA, Musunuru K. Genome Editing in Human Pluripotent Stem Cells (StemBook). 2013

Pezzini A, Granella F, Grassi M, Bertolino C, Del Zotto E, Immovilli P, Bazzoli E, Padovani A, Zanferrari C. History of migraine and the risk of spontaneous cervical artery dissection. Cephalalgia. 2005; 25:575–580. [PubMed: 16033382]

Pollock DM. Dissecting the complex physiology of endothelin: new lessons from genetic models. Hypertension. 2010; 56:31–33. [PubMed: 20516396]

Ren B, Yue F. Transcriptional Enhancers: Bridging the Genome and Phenome. Cold Spring Harb Symp Quant Biol. 2015; 80:17–26. [PubMed: 26582789]

Reschen ME, Lin D, Chalisey A, Soilleux EJ, O'Callaghan CA. Genetic and environmental risk factors for atherosclerosis regulate transcription of phosphatase and actin regulating gene PHACTR1. Atherosclerosis. 2016; 250:95–105. [PubMed: 27187934]

Kundaje A, Meuleman W, Ernst J, Bilenky M, Yen A, Heravi-Moussavi A, Kheradpour P, Zhang Z, Wang J, Ziller MJ, et al. Roadmap Epigenomics Consortium. Integrative analysis of 111 reference human epigenomes. Nature. 2015; 518:317–330. [PubMed: 25693563]

Rubinstein SM, Peerdeman SM, van Tulder MW, Riphagen I, Haldeman S. A systematic review of the risk factors for cervical artery dissection. Stroke. 2005; 36:1575–1580. [PubMed: 15933263]

Schaub MA, Boyle AP, Kundaje A, Batzoglou S, Snyder M. Linking disease associations with regulatory information in the human genome. Genome Res. 2012; 22:1748–1759. [PubMed: 22955986]

Schiffrin EL. Vascular endothelin in hypertension. Vascul Pharmacol. 2005; 43:19–29. [PubMed: 15955745]

Shi-Wen X, Denton CP, Dashwood MR, Holmes AM, Bou-Gharios G, Pearson JD, Black CM, Abraham DJ. Fibroblast matrix gene expression and connective tissue remodeling: role of endothelin-1. J Invest Dermatol. 2001; 116:417–425. [PubMed: 11231316]

Shin SY, Fauman EB, Petersen AK, Krumsiek J, Santos R, Huang J, Arnold M, Erte I, Forgetta V, Yang TP, et al. Multiple Tissue Human Expression Resource (MuTHER) Consortium. An atlas of genetic influences on human blood metabolites. Nat Genet. 2014; 46:543–550. [PubMed: 24816252]

Smemo S, Tena JJ, Kim KH, Gamazon ER, Sakabe NJ, Gómez-Marín C, Aneas I, Credidio FL, Sobreira DR, Wasserman NF, et al. Obesity-associated variants within FTO form long-range functional connections with IRX3. Nature. 2014; 507:371–375. [PubMed: 24646999]

Sorensen KE, Celermajer DS, Spiegelhalter DJ, Georgakopoulos D, Robinson J, Thomas O, Deanfield JE. Non-invasive measurement of human endothelium dependent arterial responses: accuracy and reproducibility. Br Heart J. 1995; 74:247–253. [PubMed: 7547018]

Sur IK, Hallikas O, Vähärautio A, Yan J, Turunen M, Enge M, Taipale M, Karhu A, Aaltonen LA, Taipale J. Mice lacking a Myc enhancer that includes human SNP rs6983267 are resistant to intestinal tumors. Science. 2012; 338:1360–1363. [PubMed: 23118011]

Surendran P, Drenos F, Young R, Warren H, Cook JP, Manning AK, Grarup N, Sim X, Barnes DR, Witkowska K, et al. CHARGE-Heart Failure Consortium; EchoGen Consortium; METASTROKE Consortium; GIANT Consortium; EPIC-InterAct Consortium; Lifelines Cohort Study; Wellcome Trust Case Control Consortium; Understanding Society Scientific Group; EPIC-CVD Consortium; CHARGE+ Exome Chip Blood Pressure Consortium; T2D-GENES Consortium; GoT2DGenes Consortium; ExomeBP Consortium; CHD Exome+ Consortium. Trans-ancestry meta-analyses identify rare and common variants associated with blood pressure and hypertension. Nat Genet. 2016; 48:1151–1161. [PubMed: 27618447]

Tewhey R, Kotliar D, Park DS, Liu B, Winnicki S, Reilly SK, Andersen KG, Mikkelsen TS, Lander ES, Schaffner SF, Sabeti PC. Direct Identification of Hundreds of Expression-Modulating Variants using a Multiplexed Reporter Assay. Cell. 2016; 165:1519–1529. [PubMed: 27259153]

Theodoris CV, Li M, White MP, Liu L, He D, Pollard KS, Bruneau BG, Srivastava D. Human disease modeling reveals integrated transcriptional and epigenetic mechanisms of NOTCH1 haploinsufficiency. Cell. 2015; 160:1072–1086. [PubMed: 25768904]

van de Werken HJG, Landan G, Holwerda SJB, Hoichman M, Klous P, Chachik R, Splinter E, Valdes-Quezada C, Oz Y, Bouwman BAM, et al. Robust 4C-seq data analysis to screen for regulatory DNA interactions. Nat Methods. 2012; 9:969–972. [PubMed: 22961246]

Vockley CM, D'Ippolito AM, McDowell IC, Majoros WH, Safi A, Song L, Crawford GE, Reddy TE. Direct GR Binding Sites Potentiate Clusters of TF Binding across the Human Genome. Cell. 2016; 166:1269–1281. e19. [PubMed: 27565349]

Wagner OF, Christ G, Wojta J, Vierhapper H, Parzer S, Nowotny PJ, Schneider B, Waldhäusl W, Binder BR. Polar secretion of endothelin-1 by cultured endothelial cells. J Biol Chem. 1992; 267:16066–16068. [PubMed: 1644793]

Webb TR, Erdmann J, Stirrups KE, Stitziel NO, Masca NGD, Jansen H, Kanoni S, Nelson CP, Ferrario PG, König IR, et al. Wellcome Trust Case Control Consortium; MORGAM Investigators; Myocardial Infarction Genetics and CARDIoGRAM Exome Consortia Investigators. Systematic Evaluation of Pleiotropy Identifies 6 Further Loci Associated With Coronary Artery Disease. J Am Coll Cardiol. 2017; 69:823–836. [PubMed: 28209224]

Whyte WA, Orlando DA, Hnisz D, Abraham BJ, Lin CY, Kagey MH, Rahl PB, Lee TI, Young RA. Master transcription factors and mediator establish super-enhancers at key cell identity genes. Cell. 2013; 153:307–319. [PubMed: 23582322]

Woods M, Mitchell JA, Wood EG, Barker S, Walcot NR, Rees GM, Warner TD. Endothelin-1 is induced by cytokines in human vascular smooth muscle cells: evidence for intracellular endothelin-converting enzyme. Mol Pharmacol. 1999; 55:902–909. [PubMed: 10220569]

Xu SW, Howat SL, Renzoni EA, Holmes A, Pearson JD, Dashwood MR, Bou-Gharios G, Denton CP, du Bois RM, Black CM, et al. Endothelin-1 induces expression of matrix-associated genes in lung fibro-blasts through MEK/ERK. J Biol Chem. 2004; 279:23098–23103. [PubMed: 15044479]

Yang, J., Ferreira, T., Morris, AP., Medland, SE. Madden, PA., Heath, AC., Martin, NG., Montgomery, GW., Weedon, MN., Loos, RJ., et al. Genetic Investigation of ANthropometric Traits (GIANT) Consortium; DIAbetes Genetics Replication And Meta-analysis (DIAGRAM) Consortium. Nat Genet. Vol. 44. 2012. Conditional and joint multiple-SNP analysis of GWAS summary statistics identifies additional variants influencing complex traits; p. 369-375.

Yoshizumi M, Kurihara H, Morita T, Yamashita T, Oh-hashi Y, Sugiyama T, Takaku F, Yanagisawa M, Masaki T, Yazaki Y. Interleukin 1 increases the production of endothelin-1 by cultured endothelial cells. Biochem Biophys Res Commun. 1990; 166:324–329. [PubMed: 2405848]

Zetsche B, Gootenberg JS, Abudayyeh OO, Slaymaker IM, Makarova KS, Essletzbichler P, Volz SE, Joung J, van der Oost J, Regev A, et al. Cpf1 is a single RNA-guided endonuclease of a class 2 CRISPR-Cas system. Cell. 2015; 163:759–771. [PubMed: 26422227]

Highlights

- A non-coding variant on chromosome 6 associates with five vascular diseases
- Histone acetylation shows a vascular-specific regulatory element at the causal SNP
- Genome editing at the SNP demonstrates distal regulatory effect on endothelin-1
- Endothelin-1 signaling in blood vessels may explain pattern of vascular disease risk

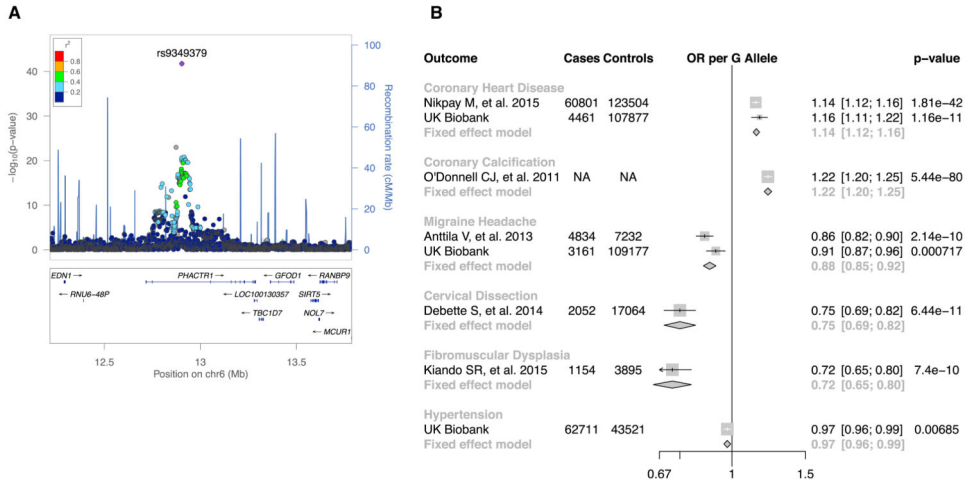

Figure 1. Lead SNP in 6p24 Locus, rs9349379, Is Associated with Multiple Vascular Diseases

(A) Locus Zoom Plot of 6p24 associations for CAD/MI. Each variant identified in 1000 Genomes Project sequencing is represented by a dot, with color representing linkage disequilibrium (LD) with the lead SNP. A single variant, rs9349379, demonstrates the most significant association with CAD/MI ($p = 1.81 \times 10^{-41}$). No variants in the locus are in significant LD with rs9349379 ($r^2 > 0.5$).

(B) Multiple disease associations of rs9349379 minor allele (G) with vascular disorders. The minor allele (G) is associated with increased risk of CAD and coronary calcification. The minor allele is alternatively associated with reduced risk of cervical dissection, migraine headache, fibromuscular dysplasia, and hypertension. CAD and migraine headache associations are confirmed in UK Biobank data.

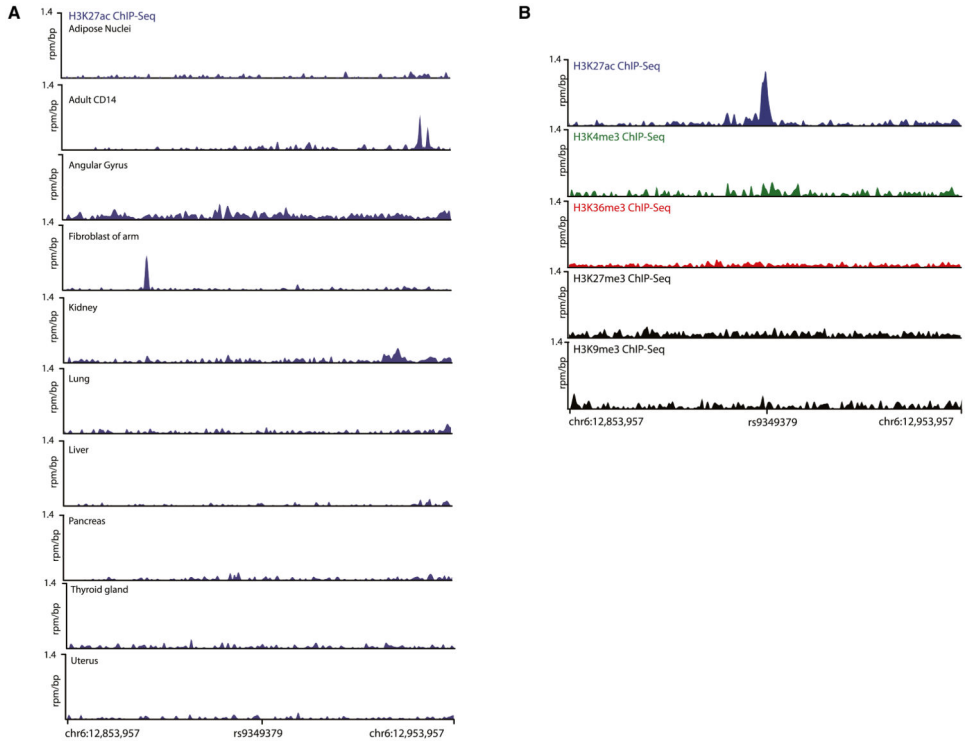

Figure 2. H3K27 Acetylation Identifies a Vascular-Specific Regulatory Element at rs9349379

(A) Chromatin immunoprecipitation sequencing (ChIP-seq) for H3K27Ac signal at the 6p24 locus shows no evidence of an enhancer or promoter element within 100 kb of rs9349379 in non-vascular tissues.

(B) Arterial tissue from the Aorta shows a strong H3K27Ac peak at rs9349379, with no signal at the locus for H3K4me3, H3K36me3, H3K27me3, or H3K9me3. All data are plotted as rpm/bp for ChIP-seq conducted in one representative tissue sample of each type.

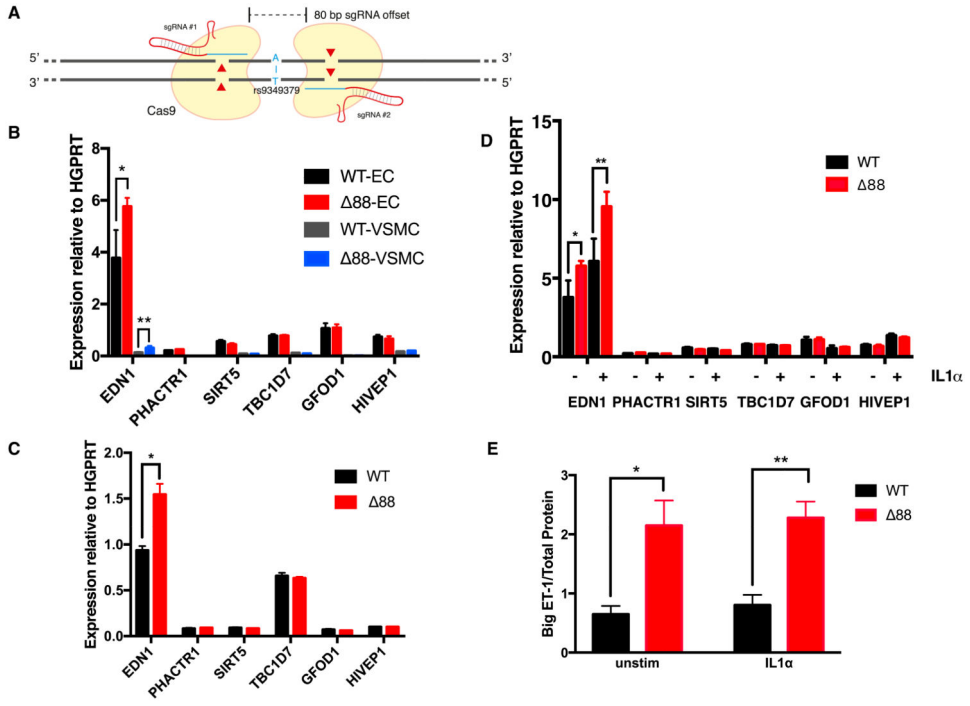

Figure 3. Targeted Deletion at 6p24 Causal SNP Increases EDN1 Expression in Stem Cell-Derived Vascular Cells

(A) Generation of cell lines with 88-bp deletion at rs9349379, with two sgRNAs flanking the rs9349379 regulatory region.

(B) iPSC-derived ECs and VSMCs have increased *EDN1* expression after deletion of the rs9349379 regulatory region (Δ88) with flanking CRISPR/Cas9 nucleases. Other genes in the 6p24 locus are minimally expressed and are not significantly altered (*p = 0.028 and **p = 0.01).

(C) ESC-derived ECs have increased *EDN1* expression with Δ88 deletion (*p = 0.0004).

(D) *EDN1* expression increases in both WT and Δ88 iPSC-ECs in response to IL-1α stimulation (50 ng/mL) (*p = 0.03 and **p = 0.005).

(E) Increased Big ET-1 protein level before and after IL-1α stimulation in Δ88 iPSC-derived ECs (*p = 0.003 and **p = 0.0004). All data represent mean ± SEM of three independently differentiated clones in each group.

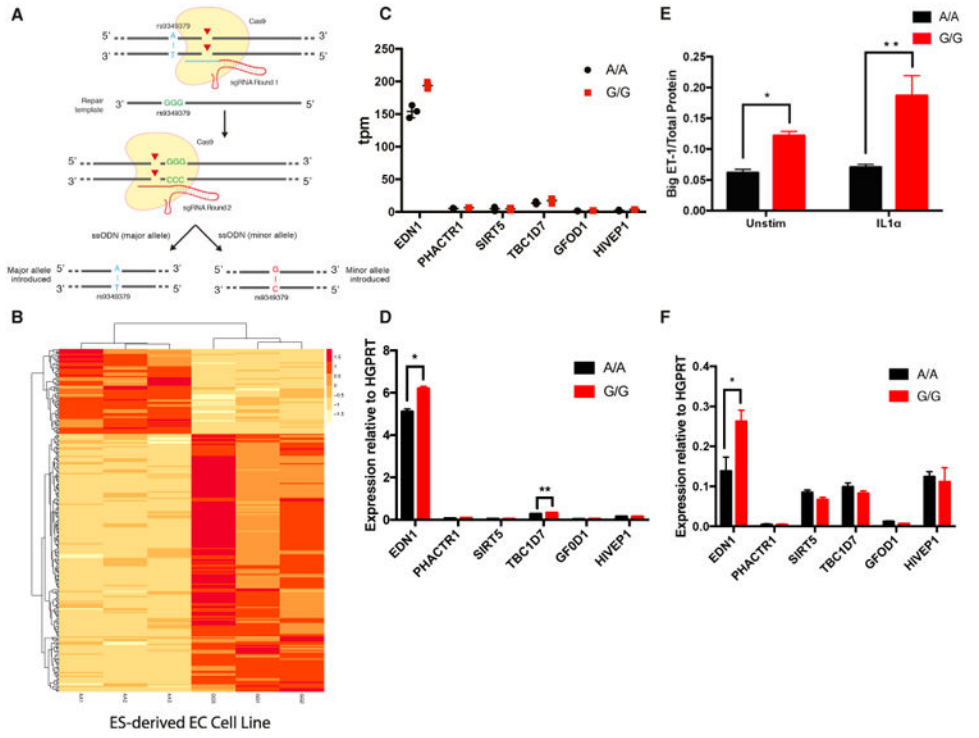

Figure 4. Allelic Series at rs9349379 Demonstrates *cis*-Regulatory Effect on *EDN1* Expression

(A) Generation of an allelic series of stem cell lines at rs9349379. A heterozygous stem cell line (Hues66) was edited to first insert PAM sites, and then it was edited in a second round to generate three homozygous clones for both the major (A) and minor (G) alleles.

(B) Differential gene expression analysis of RNA-seq from AA versus GG ESC-derived ECs shows 273 differentially expressed transcripts (FDR < 0.05), with clustering by genotype at rs9349379.

(C) RNA-seq expression for genes in the 6p24 locus demonstrates significantly increased expression of *EDN1* in G/G ESC-derived ECs compared with A/A isogenic control. Other locus genes show minimal expression in transcripts per million reads (tpm).

(D) The qPCR in separately differentiated ESC-ECs validates the expression difference for *EDN1* (*$p = 7.59 \times 10^{-7}$) and *TBC1D7* (**$p = 1.75 \times 10^{-5}$).

(E) Increased Big ET-1 expression before and after IL-1α stimulation in homozygous minor (G/G) ESC-derived ECs (*$p = 2.12 \times 10^{-5}$ and **p = 0.0006).

(F) Homozygous minor ESC-derived VSMCs demonstrate higher expression of *EDN1* (*p = 0.012), while no other 6p24 locus genes show differential expression.

All data represent mean ± SEM of three independently differentiated clones of each genotype.

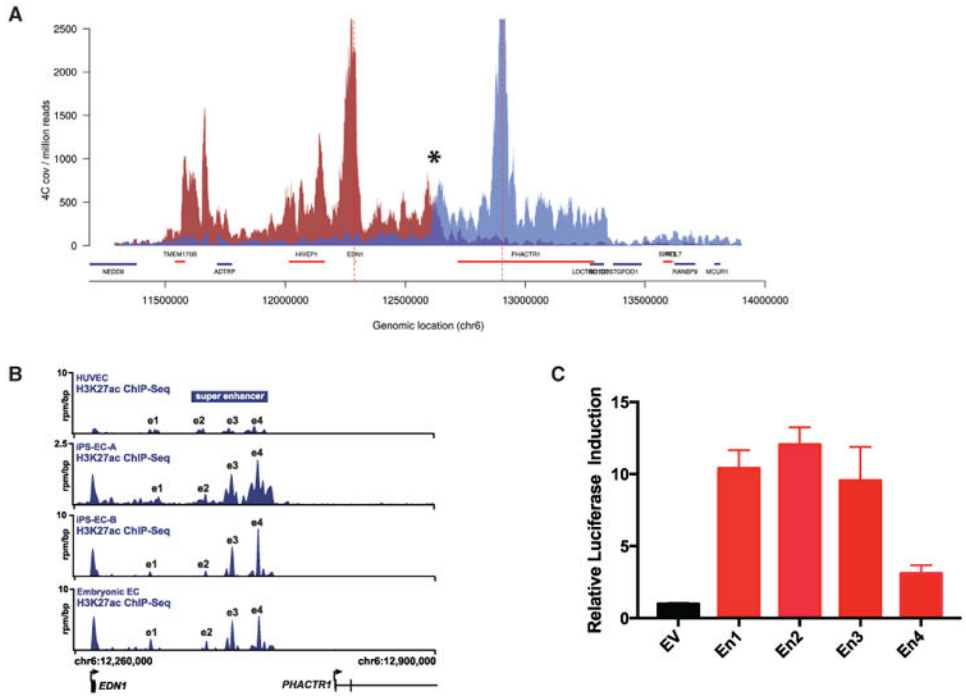

Figure 5. Very Low Contact between *EDN1* Promoter and rs9349379 by 3D Chromatin Structure

(A) 4C-seq in human coronary artery ECs demonstrates 3D chromatin loops from the *EDN1* promoter viewpoint (red) and rs9349379 SNP viewpoint (blue). The *EDN1* promoter contacts multiple sites extending up to 500 kb in both the 3′ and 5′ directions. 4C-seq from the rs9349379 viewpoint demonstrates a smaller contact region that extends from chr6:12,690,000 to 13,350,000. There is a common contact area intergenic to *EDN1* and PHACTR1 (*).

(B) Super enhancer at chr6:12,490,000–12,590,000 seen in H3K27Ac ChIP-seq in human umbilical vein endothelial cell (HUVEC), iPSC-derived EC, and embryonic-derived EC. The super enhancer is within the same transcriptionally associated domain as *EDN1*, and it also includes the common contact sites of the *EDN1* promoter and rs9349379 regulatory element. HUVEC, iPSC-EC-B, and embryonic-EC were generated from publicly available data.

(C) Demonstration of strong enhancer activity for each of the four discrete regions that comprise the super enhancer. The 2-kb segments were tested in a luciferase expression assay and compared with empty vector (EV); each region had a 2- to 12-fold induction of luciferase signal.

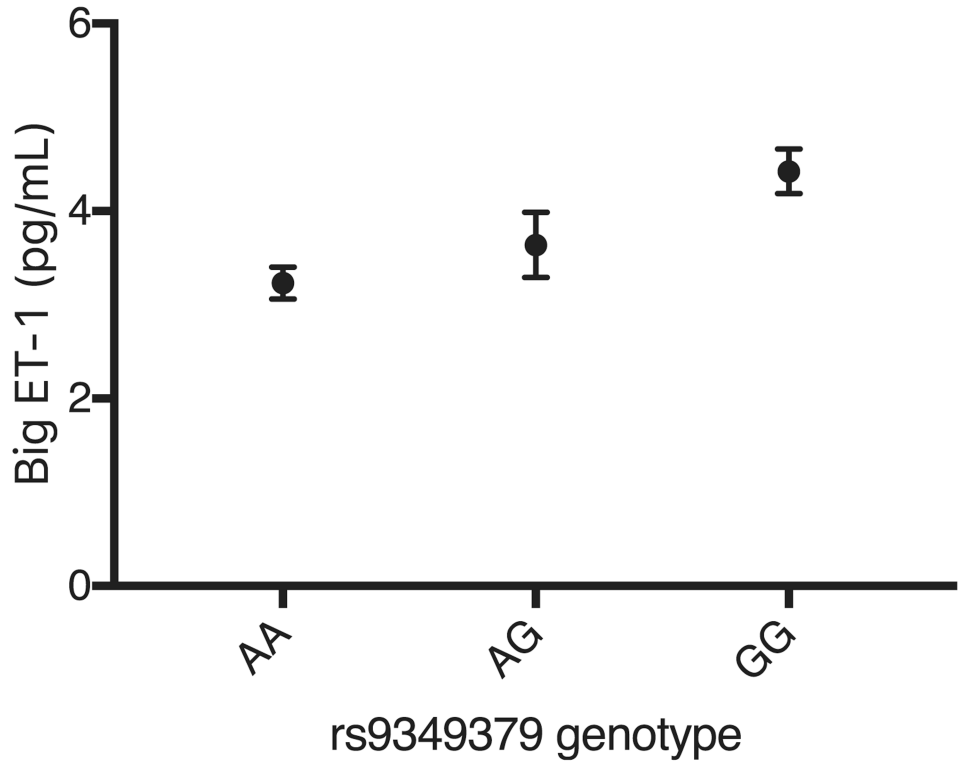

Figure 6. Minor Allele at rs9349379 Increases Plasma Levels of Big ET-1 in Healthy Subjects

Association between circulating levels of ET-1 precursor protein and genotype at rs9349379 in human plasma samples. Each copy of G allele results in higher Big ET-1 expression (n=33 for each rs9349379 genotype; p = 0.00136, additive model of regression).

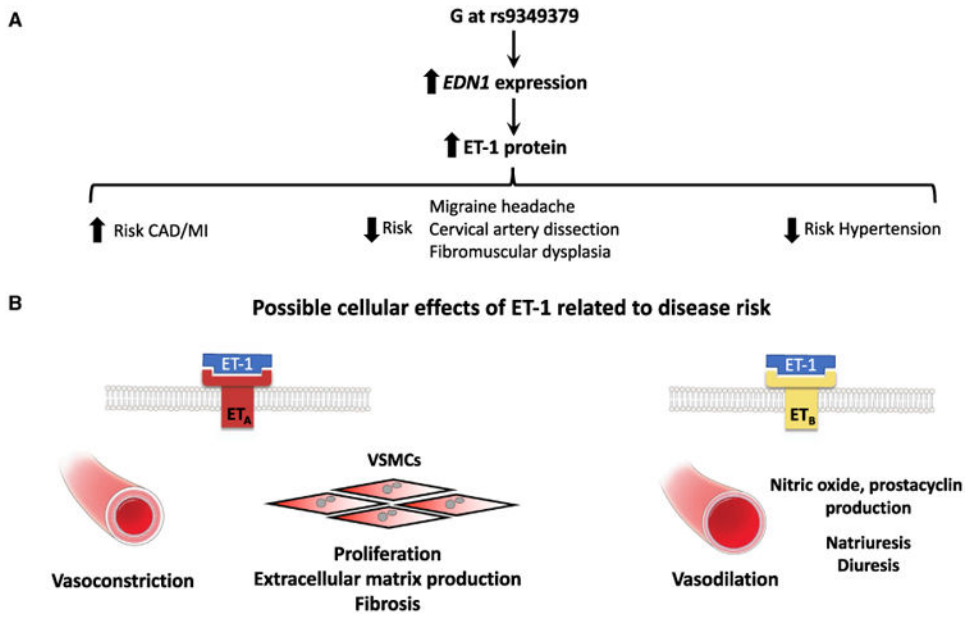

Figure 7. The Relationship between rs9349379 Genotype, Endothelin-1, and Risk of Five Vascular Diseases

(A) The *cis*-regulatory effect of the G allele at rs9349379 is associated with higher *EDN1* expression and higher ET-1 secreted protein. The G allele at rs9349379 is associated with increased risk of CAD/MI and lower risk of migraine headache, cervical artery dissection, fibromuscular dysplasia, and hypertension.

(B) Proposed model for ET-1 function and risk of five vascular diseases. Activation of ET_A receptor results in vasoconstriction, VSMC proliferation, ECM production, and fibrosis. These downstream effects of ET-1 result in increased risk of CAD/MI and decreased risk of migraine headache, cervical artery dissection, and fibromuscular dysplasia. ET_B receptors are predominantly in large arteries and the renal collecting system. Higher ET-1 levels may result in hypotension via ET_B-induced nitric oxide and prostacyclin production, resultant vasodilation, diuresis, and natriuresis.

Key Resources Table

REAGENT or RESOURCE	SOURCE	IDENTIFIER
Antibodies		
H3K27Ac (39133, Active Motif)	Active Motif	Cat#: 39133
Bacterial and Virus Strains		
MAX Efficiency DH5α Competent Cells	ThermoFisher Scientific	Cat#: 18258012
One Shot Stbl3 Chemically Competent *E. coli*	ThermoFisher Scientific	Cat#: C737303
Biological Samples		
Human Plasma Samples	Partners Healthcare Biobank	N/A
Chemicals, Peptides, and Recombinant Proteins		
Accutase	StemCell Technologies	Cat#: 07920
mTeSR1	Stem Cell Technologies	Cat#: 85850
ROCK Inhibitor Y-27632	Santa Cruz	Cat#: sc-281642
Geltrex	ThermoFisher Scientific	Cat#: A1413202
VascuLife VEGF Endothelial Medium	Lifeline Cell Tech	SKU: LL-0003
2-Mercaptoethanol	Sigma Aldrich	CAS#: 60-24-2
N2 Supplement	Invitrogen	Cat#: 17502048
B27 Supplement	Invitrogen	Cat#: 17504044
DMEM/F12	ThermoFisher Scientific	Cat#: 11320033
Neurobasal Medium	ThermoFisher Scientific	Cat#: 21103049
StemPro-34 SFM medium	Invitrogen	Cat#: 10639011
CHIR-99021	Cayman Chemical	CAS#: 252917-06-9
BMP4	R&D Systems	Cat#: 314-BP
VEGF165	PeproTech	Cat#: 100-20
Forskolin	Sigma-Aldrich	CAS#: 66575-29-9
CD-144 Microbeads	Sigma-Aldrich	SKU: V1514
Knockout Serum Replacement	ThermoFisher Scientific	Cat#: 10828028
Glutamax	ThermoFisher Scientific	Cat#: 35050061
MEM-NEAA	ThermoFisher Scientific	Cat#: 11140050
Insulin	Sigma Aldrich	CAS#: 11061-68-0
Knockout DMEM	ThermoFisher Scientific	Cat#: 10829018
HEPES	ThermoFisher Scientific	Cat#: 15630080
bFGF	R&D Systems	Cat#: 233-FB-025
LDN-13189	Stemgent	Cat#: 04-0074
SB431542	Tocris	CAS#: 301836-41-9
TRIzol	Life Technologies	Cat#: 15596026
PMSF	Cell Signaling	CAS#: 329-98-6

REAGENT or RESOURCE	SOURCE	IDENTIFIER
IL1alpha	PeproTech	Cat#: 200-01-A
protein G Dynabeads	Life Technologies	Cat#: 10004D
AMPure beads	Beckman-Coulter	Part#: A63880
PFU Ultra II HS PCR mix	Agilent	Cat#: 600850
CD14 MicroBeads	Miltenyi	Cat#: 130-050-201
FuGene6	Promega	Cat#: E2691
Viafect	Promega	Cat#: E4982
Bicinchoninic acid (BCA) Protein Assay	ThermoFisher Scientific	Cat#: 23227
DpnII	New England Biolabs	R0543L
Csp6I	Thermofisher	ER0211
T4 Ligase	Roche	10799009001
Nucleomag P-beads	Clontech	744 100.24
Critical Commercial Assays		
Big-ET1 ELISA Assay	Enzo Life Sciences	Product #: ADI-900-022
Dual-Luciferase Reporter Assay System	Promega	Cat#: E1910
Deposited Data		
RNA sequencing (AA1, AA2, AA3, GG1, GG2, GG3 samples)	Mendeley	http://dx.doi.org/10.17632/z259mb2tvy.1,
		http://dx.doi.org/10.17632/9frfyyhdc2.1
		http://dx.doi.org/10.17632/9hccrsn9s3.1,
		http://dx.doi.org/10.17632/xhhvsm9r5k.1
ChIP-seq BAM files: iPSC-ECs	Mendeley	http://dx.doi.org/10.17632/jznmppxyrd.1
Experimental Models: Cell Lines		
Human: 1016 hiPSC line	HSCI iPS Core	N/A
Human: HUES 9 hESC line	HSCI iPS Core	N/A
Human: HUES 66 hESC line	HSCI iPS Core	N/A
Human Coronary Artery Endothelial Cell Line	Lifeline Cell Technology	FC-0032
Human Aortic Endothelial Cell Line	Lifeline Cell Technology	FC-0014
Human: Primary Monocyte Cell Line	Leukopacs, MGH Blood Bank	N/A
Human: Embryonic Kidney 293 Cell Line	ATCC	CRL-1573
Oligonucleotides		
PHACTR1 (Hs01116214_m1)	Life Technologies	Cat#: 4331182
EDN1 (Hs00174961_m1)	Life Technologies	Cat#: 4331182
TBC1D7 (Hs00212898_m1)	Life Technologies	Cat#: 4331182
SIRT5 (Hs00978335_m1)	Life Technologies	Cat#: 4331182
HIVEP1 (Hs00172428_m1)	Life Technologies	Cat#: 4331182
GFOD1 (Hs00255879_m1)	Life Technologies	Cat#: 4331182

REAGENT or RESOURCE	SOURCE	IDENTIFIER
Human HPRT1 (HGPRT) Endogenous Control (VIC/ TAMRA)	Life Technologies	Cat#: 4310890E
sgRNA sequences:		
5′ Δ88 Guide1	Integrated DNA technologies	TTAAGAAGCATGAGTAAAA
3′ Δ88 Guide 2	Integrated DNA technologies	CGTGGAAAATATAACTA
Precise editing, round 1	Integrated DNA technologies	CGTGGAAAATATAACTA
Precise editing, round 2-A	Integrated DNA technologies	TGCCCTTGAGATCATATAA
Precise editing, round 2-B	Integrated DNA technologies	GCCCTTGAGATCATATAAA
Precise editing, round 2-C	Integrated DNA technologies	TAGCCAATGATTTTAAGCT
Precise editing, round 2-D	Integrated DNA technologies	ATAGCCAATGATTTTAAGC
Recombinant DNA		
pGL4-SV40 vector	Promega	pGL4.13[*luc2*/SV40]
Plasmid: PX459v2	Addgene	pSpCas9(BB)-2A-Puro (PX459) V2.0
Software and Algorithms		
R software package	R project	https://r-project.org
PLINK software package	Purcell Lab	http://zzz.bwh.harvard.edu/plink/
Kallisto/Sleuth software for RNA-seq analysis	Pachter Lab	https://pachterlab.github.io/kallisto/download http://pachterlab.github.io/sleuth/about
BAMPlot	Lin Lab	https://github.com/linlabbcm/bamplot
Integrative genomics viewer	Broad Institute	http://software.broadinstitute.org/software/igv/
Model-based analysis for Chip-seq (MACS)	Liu Lab	http://liulab.dfci.harvard.edu/MACS/
Rank ordering of super-enhancers (ROSE)	Young Lab	http://younglab.wi.mit.edu/super_enhancer_code.html
Graphpad Prism	Graphpad	www.graphpad.com/scientific-software/prism/
FourCSeq (R package)	Huber Lab	http://bioconductor.org/packages/release/bioc/html/FourCSeq.html